Distribution of desferrioxamine-B-extractable soluble manganese(III) and particulate MnO_2 in the St. Lawrence Estuary, Canada

Matthew R. Jones [a†‡], Véronique E. Oldham [b*], George W. Luther [b], Alfonso Mucci [c], Bradley M. Tebo [a]

[a] Division of Environmental and Biomolecular Systems, Oregon Health & Science University, Portland, OR 97239, USA

[b] School of Marine Science and Policy, University of Delaware, Lewes, DE 19958, USA

[c] GEOTOP and Department of Earth and Planetary Sciences, McGill University, Montreal, QC H3A 0E8, Canada

current addresses:

[†] POSTECH – Pohang University of Science and Technology, Division of Environmental Science and Engineering, Pohang-si, Gyoungsangbuk-do, 37673, Korea

* WHOI – Woods Hole Oceanographic Institute, Department of Marine Chemistry and Geochemistry, Woods Hole, MA 02543, USA

[‡]corresponding author

Abstract

Soluble organically-complexed manganese(III) (Mn(III)–L) is an intermediate species in the manganese cycle. The reactivity of the complex(es) depends on the abundance and nature of the ligand(s), as well as its physicochemical environment. Currently, the strength of Mn(III)-L complexes is assessed by their ability to react either directly with a porphyrin complex, using the kinetics of its competitive ligand exchange reactions, or after being reduced to manganese(II). We present a new three-step technique that quantifies part of the Mn(III)-L pool which may represent a bioavailable and reactive fraction of the complexes. This technique relies on 1) ligand exchange of the dissolved complexes in a filtered field sample with the siderophore desferrioxamine-B (DFOB), 2) chromatographic separation and concentration of manganese(III)-DFOB from the aqueous matrix, and 3) quantification of the naturally ligated manganese(III) that was outcompeted by DFOB (Mn(III)-L_{DFOB}) at low concentrations by flow injection UV-Vis spectrophotometry. The formation of an extractable Mn(III)-L_{DFOB} complex provides an operationally-defined benchmark by which to assess biological interactions and better understand the cycling of manganese(III) in the environment. The technique, with a detection limit of 0.09 nM, was applied to water samples collected in the St. Lawrence Estuary (SLE) and adjacent Saguenay Fjord in Canada. Mn(III)-L_{DFOB} was ubiquitous at our study sites, but its concentration was low relative to total dissolved manganese (dMn_T) and particulate MnO_2. Spatial variations of the dMn_T speciation within the Saguenay Fjord suggest that Mn(III)-L forms from the reduction of MnO_2. Likewise, variations of the dMn_T speciation along a dissolved oxygen gradient in the SLE leads us to believe that Mn(III)-L_{DFOB} likely represents a fraction of the total Mn(III)-L that cycles more readily in estuarine and marine systems.

1.0 Introduction

Manganese is commonly found in three oxidation states in aquatic environments, cycling between two end-member species, soluble manganese(II) and particulate manganese(III,IV) oxides (MnO_x). Nevertheless, there is an underlying complexity to the aquatic manganese cycle as the intermediate oxidation state, manganese(III), can also occur as a soluble complex (Mn(III)-L, where L denotes a complexing ligand). Mn(III)-L is present in significant concentrations in oxic and suboxic/anoxic stratified marine waters (Schnetger and Dellwig, 2012; Trouwborst et al., 2006; Yakushev et al., 2007), sediment porewaters (Madison et al., 2013, 2011) as well as estuarine (Oldham et al., 2015, 2017b, 2017a) and freshwater (Dellwig et al., 2012) environments.

Organic ligands that can complex manganese(III) range in both strength and coordination number with Mn^{3+}. Hence, Mn(III)-L complexes may display differential geochemical behaviors according to the nature of the ligand. For example, manganese centers in photosystem II are responsible for the oxidation of water to oxygen (Zouni et al., 2001). Mn(III)-L complexes have an implied ability to degrade recalcitrant carbon (Glenn et al., 1986; Perez and Jeffries, 1992; Schlosser and Höfer, 2002) as well as oxidize reduced sulfur and nitrogen compounds (Klewicki and Morgan, 1999, 1998; Kostka et al., 1995; Luther et al., 1999) and various organic contaminants (Sun et al., 2015). Natural MnO_x will oxidize high molecular weight organic material, such as humic substances, producing low molecular weight compounds (Sunda and Kieber, 1994), with their concomitant reduction to manganese(III) or manganese(II). The resultant low molecular weight organic compounds include known compounds, such as malate, oxalate and pyruvate, that complex and stabilize manganese(III) in solution (Magliozzo and Marcinkeviciene, 1997; Stone, 1987; Stone and Morgan, 1984; Wariishi et al., 1992; Xyla et al., 1992). In spite of the known, distinctive stability of different Mn(III)-L complexes, relatively little is known about the processes and the nature of the ligands that form these complexes in the environment.

The relative strength of dissolved Mn(III)-L complexes can be defined according to the exchange rate of manganese(III), with a cadmium substituted porphyrin complex, α,β,γ,δ-tetrakis(4-carboxyphenyl)porphine (Luther et al., 2015; Madison et al., 2013, 2011), if exchange occurs within a 15-minute period these are termed weak complexes. If, following addition of a reductant

to the sample and porphine complex, there is a further exchange of manganese this pool is denoted as a strong complex (Luther et al., 2015; Oldham et al., 2017a, 2017b, 2015). The well-characterized siderophore, desferrioxamine-B (DFOB) is used as the model ligand, Log K_{COND} = 13.2, to differentiate between strong and weak manganese(III) complexes (Luther et al., 2015; Oldham et al., 2017b, 2017a, 2015). Oldham et al. (2017b, 2017a) found that strong ligands binding to manganese(III) (log K_{COND} >13.2) in estuarine environments, were most likely terrestrial humic material. These complexes were not readily labile and their quantification was based on the difference in the absorbance of the sample upon reaction with the porphyrin, before and after the addition of hydroxylamine and heat treatment for 1 hour at 90 °C. The reduction of manganese(III) to manganese(II) enables manganese to more readily substitute for cadmium in the porphyrin. Manganese(III), likely stabilized by terrestrial humic complexes, has been found in both the river waters feeding and throughout a drinking water treatment works (Johnson et al., 2018). Manganese(III) has also been found in low oxygen marine environments (Trouwborst et al., 2006; Schnetger and Dellwig, 2012; Yakushev et al., 2007) rich in polyphosphate complexes (Yakushev et al., 2009). Siderophores, known to complex iron(III) in solution, can also stabilize manganese(III) (Duckworth and Sposito, 2005; Faulkner et al., 1994; Heintze and Mann, 1947; Parker et al., 2007, 2004), sometimes forming complexes with similar or greater kinetic stability than iron(III) complexes (Luther et al., 2015; Parker et al., 2004).

Desferrioxamine-B (DFOB) is a strong, hydroxamate manganese(III)-binding ligand with a stability constant similar to that of iron(III) (Duckworth and Sposito, 2005). Its strength and the likely formation of manganese(III) hydroxamate complexes in the environment suggest that DFOB may be a good model compound against which to operationally characterize biological interactions with weak Mn(III)-L complexes including other siderophores. Environmental Mn(III)-L complexes that can undergo a fast ligand exchange with α,β,γ,δ-tetrakis(4-carboxyphenyl)porphine (i.e. weak ligands) are also highly likely (95 % confidence) to undergo ligand exchange with DFOB (Madison et al., 2011). Though Mn(III)-L complexes may be made labile through a variety of processes, including photochemical reactions if using iron(III) as an analogue (Barbeau et al., 2003), Mn(III)-L complexes much stronger than Mn(III)-DFOB are likely to be more inert to biooxidation or bioreduction whereas weaker Mn(III)-L complexes should be bioavailable. This hypothesis is supported by recent laboratory studies with manganese(II)-oxidizing *Pseudomonas* species that can oxidize Mn(III)-DFOB complexes, but at

a reduced rate and extent compared to manganese(II) and weaker Mn(III)-L complexes (Wright et al., 2018). Thus, the strength of the Mn(III)-DFOB complex provides an operationally defined benchmark to better understand the cycling of manganese(III) in the environment.

The method we present here is adapted from Trouwborst et al. (2006). It uses DFOB (log K_{COND} = 13.2 in seawater (Luther et al., 2015); log $K_{[Mn(III)HDFOB+]}$ = 28.6 ± 0.5 in 0.1 M NaCl (Duckworth and Sposito, 2005)) to outcompete the natural, stabilizing ligand in the Mn(III)-L complex present in a filtered sample and to concentrate it on a solid phase extraction column. Application of this method, with a sub-nanomolar detection limit, provides insights into the amount of manganese(III) complexed by natural organic compounds whose formation constants are less than or equal to that of DFOB. Results of the method were combined with measurements of MnO_2 determined in terms of particulate manganese oxidizing equivalents (in contrast to most measurements in aquatic systems that characterize total particulate manganese) and total dissolved manganese (dMn_T) to better constrain the behavior of this component of the manganese cycle in the St. Lawrence River Estuary (Fig. 1).

2.0 Methods

2.1 Components

Sample extraction (protocol, Fig. 2) and flow injection analysis UV-Vis spectrophotometry (FIA-S: protocol, Fig. 2; schematic, Fig. 3) were carried out using an Ismatec, 16-channel, peristaltic pump. During sample extraction, Oasis cartridges were connected to Tygon E-LFL, 1.14 mm internal diameter (id), peristaltic pump tubes. During FIA-S, 4 × 0.38 mm id (reagents) and one 0.76 mm id (sample) PVC peristaltic pump tubes were used. All other FIA-S tubing was 1.6 mm id Teflon, including the three mixing tubes, two 1.2 m long and one 3.6 m long. Mixing tubes were connected through y-shaped polyether ether ketone fittings (PEEK; Upchurch Scientific). A manually-controlled, 6-port, 2-position, Cheminert, Valco Instruments Company Incorporated (VICI) valve was used to switch between loading and eluting samples from the 18 µL column (Global FIA). Quantification of samples during FIA-S used a World Precision Incorporated (WPI) 100-cm liquid wave capillary cell (LWCC). Either the 1-cm cell holder or the 100-cm LWCC were connected through optical fiber cables to an Ocean Optics USB2000

spectrophotometer with halogen light source (HL-200-FHSA). Other spectrophotometric analyses were conducted on a SpectraMax M2 plate reader with UV capability.

2.2 Reagents

All reagents, unless specified, were prepared in 18.1 MΩ de-ionized water (DI). Mn(III)-L complexes and δ-MnO_2, used for method development, were synthesized according to procedures provided in the Supplementary Material. DFOB (mesylate salt, Sigma) solutions in DI should be as fresh as possible, as DFOB loses complexing activity over time (Duckworth and Sposito, 2005), we used solutions aged a maximum 3-5 days. The chromatography stationary phases were Oasis Hydrophilic-Lipophilic-Balanced (HLB; Waters) and Tosoh Toyopearl AF-Chelate-650 M (Sigma). Oasis HLB was obtained in prepacked cartridge form. Reagent stocks used for washing and priming the Oasis HLB were 10 % w/v hydroxylamine hydrochloride (NH_2OH-HCl; trace metal grade, Fisher) and 1 M 4-(2-hydroxyethyl)piperazine-1-ethanesulfonic acid (HEPES; Sigma) at pH 7.8.

Reagents for FIA-S were 0.2 M Tiron (1,2-dihydroxybenzene-3,5-disulfonate, Sigma) and 0.2 M H_2O_2 (50 % stabilized, Fisher) solutions prepared in 0.25 M borax buffer at pH 8.7 (27.24 g $Na_2B_4O_7.10H_2O$ (Fisher) and 11.04 g H_2BO_3 (Fisher) per 1000 mL). The same borax buffer was used to prepare 0.2 M 2,2'-dipyridyl (Acros Organics) in 50 % v/v borax/methanol (Chromasolv, Sigma). The Tiron working reagent was an equimolar concentration of Tiron and 2,2'-dipyridyl diluted into the borax buffer. The analytical buffer was 0.22 M borax at pH 10.5 (750 mL of 0.25 M borax (pH 8.7) and 120 mL of 22 % ammonium hydroxide (20-22 %; trace metal grade, Fisher)). The eluting acid was 0.4 M HCl (trace metal clean). The pH of acidified samples was adjusted through the addition of a 0.5 M ammonium borate, $(NH_4)_3BO_3$, solution (pH 9.4; 15.46 g of H_2BO_3 with 22.94 mL of 20-22 % trace metal clean NH_4OH made up to 500 mL). A dilution of this buffer to 0.05 M (pH 9.2) was used to rinse/prepare the AF-Chelate-650M column. Manganese(II) sulfate (Sigma) used for standards was dried at 50 ˚C overnight before being weighed and dissolved in DI. Diluted standards were acidified as per samples (Section 2.4.2) and used to calibrate the technique (Fig. 3) through the Tiron absorbance measured at 424 nm.

2.3 Locations, oceanography and sampling

Water column samples were collected at four locations in September 2014, two in the Saguenay Fjord, one in the Lower St. Lawrence Estuary and one in the Gulf of St. Lawrence (Fig. 1 and Table 1). Additionally, a surface water transect was sampled in the Saguenay Fjord, a tributary of the St. Lawrence Estuary, with samples being taken as the ship transited seaward from Station SAG05 (time 08:00 EST) to SAG48 (time 15:05 EST).

Stations 23 and 17 are situated within the deep (>300 m) Laurentian Channel whose water column is characterized by a three-layer structure. Surface (0-20 m, but up to 50 m; salinity (S_p) ~20-33) waters carry freshwater from the St. Lawrence River and flow seawards towards the Atlantic. The cold intermediate layer (CIL; 20-200 m, σ_θ ~23.8-27), that originates in the Gulf of St Lawrence in the winter, flows landward, and deep (200 m - bottom, σ_θ ~27-27.2) waters, from the Atlantic, also flow landward (Saucier et al., 2003). Because of the steep sill at the head of the Laurentian Channel, the CIL and the deep waters are forced to upwell. Episodically, CIL waters overflow the ~22 m sill and enter the Saguenay Fjord, typically sinking and filling the fjord's inner and outer basins (Belzile et al., 2016).

The Saguenay Fjord is up to 275 m deep, 110 km long and has an average width of 2 km. The Saguenay River is the main outlet from the Saint-Jean Lake and the most influential tributary to the fjord. The overflow and the intrusion of marine waters from the St. Lawrence Estuary generate a sharp halocline, leading to a simplified two-layer water stratification: a thin brackish surface layer (5-10 m, S_P ~10) overlying a denser layer (S_p ~30) of marine waters. The fjord surface waters discharge into the main estuary; the plume formed by these waters during low tide can be found in the LSLE up to 10 km from the mouth of the fjord and be detected at a depth of up to 25 m (Lebel et al., 1983; Mucci et al., 2017).

All samples were collected using a rosette system (12 × 12 L Niskin PVC bottles) equipped with a Conductivity-Temperature-Depth sensor (CTD, Seabird SBE-911). Samples were collected directly from the Niskin bottles into acid-cleaned 250 mL polycarbonate bottles (cleaning protocol is provided in the Supplementary Material), being filled to the brim (265 mL) after rinsing three times. Samples were stored in the dark at 4 °C, and filtered (0.2 μm Whatman Nuclepore track-etched polycarbonate membranes) within 20 minutes. All polysulfone filtration units and sample tubes were rinsed three times either with the sample or filtrate, as required.

2.4 Ancillary analytes

2.4.1 Particulate MnO_2

A 97 mM (4 % w/v) leucoberbelin blue (LBB, Sigma) stock solution was adjusted to pH 10.5 by adding a small volume of NH_4OH (final concentration 26 mM). Previous laboratory work indicated that this solution is stable, in the dark at 4 °C, for at least 1 year. The precipitate that forms during refrigeration must be re-dissolved by warming the solution to room temperature. The LBB primary reagent is 974 μM (0.04 % w/v) LBB in 17.5 mM (1 %) acetic acid (trace metal grade, Fisher); the working reagent is a dilution of the primary reagent to 77.6 μM LBB. A calibration curve for LBB is generated using $KMnO_4$ (Sigma) in DI. The reduction of $KMnO_4$ to manganese(II) stoichiometrically oxidizes 5 LBB molecules, so calibration curves are corrected based on the oxidizing equivalents of the manganese, with particulate manganese assumed to be MnO_2. The assumption that all environmental MnO_x is MnO_2 is debatable, but commonly reasonable. Manganese oxidation is mostly mediated by bacterial processes (Tebo and Emerson, 1986) and, when coupled with secondary (surface) oxide formation, the resultant mineral phases contains <10 % manganese(III) (Bargar et al., 2005). The LBB assay for MnO_2 is unreactive towards manganese(II) (Krumbein and Altmann, 1973), so what is measured is the average manganese(III/IV) (Zhu et al., 2017). It should be noted, however, that Murray et al. (1984) found that LBB could overestimate the manganese oxidation state and attributed this to a surface catalyzed air oxidation of LBB. Based on the LBB oxidation stoichiometry, if the MnO_2 contains 10 % manganese(III) it introduces an error of -5 % in the estimate of MnO_2.

For the analysis of MnO_2, the sample filters were placed in polypropylene tubes to which 2 mL of the LBB working reagent was added and the samples were shaken. If, after 1-hour, the solution's coloration was too high, additional working reagent was added – samples were periodically shaken before analysis 12 hours later. The absorbance of the blue colored oxidized LBB was measured using a 1-cm path length cuvette at 624 nm. A baseline correction is calculated from the slope of the linear regression between the absorbance at 480 and 700 nm. The error on the LBB measurement is taken from the relative standard deviation of the standards (<2 %), as this was higher than the error on the repeat measurements of the sample. The

analytical range achievable with a 1-cm cell is 0.3 to 25 μM and the limit of detection is 130 nM which, when corrected for the volume passed through the filter, was 1 nM.

2.4.2 Total dissolved manganese

Total dissolved manganese (dMn_T) was only determined on samples collected in the Saguenay Fjord. Following filtration, small volumes of NH_2OH-HCl were added to 15 mL aliquots of the samples, to a final concentration of 14.7 μM. Samples were stored cold (4 °C) for 14 days before addition of 4 μL 6 M HNO_3 (Optima; Fisher) per 1 mL sample for further storage at 4 °C. The samples were diluted ten-fold with 1 % HNO_3 prior to analysis on an Agilent 7700 inductively coupled plasma–mass spectrometer (ICP-MS). The recovery of the National Research Council of Canada certified reference material, for trace metals in estuarine water, SLEW-3 (S_p ~33 and dMn_T = 29.5 ± 4 nM) was 28.6 ± 2.8 nM. The blank for dMn_T was 0.2 μm filtered DI with additions of NH_2OH-HCl and HNO_3, as per the samples. The formaldoxime method (Brewer and Spencer, 1971) was used to quantify soluble manganese during experimental work, this method is presented in the Supplementary Material.

2.5 Manganese(III)

Following the filtration of field samples, the determination of dissolved manganese(III) using the DFOB extraction relied on 3 steps. 1. Exchange of manganese(III) from Mn(III)-L to DFOB. 2. Extraction of Mn(III)-DFOB from the sample and its reduction to manganese(II). 3. Quantification of soluble manganese, either as Mn(III)-DFOB or manganese(II), across a range of concentrations.

During laboratory validation of the method, the direct quantification of Mn(III)-DFOB and other manganese(III)-complexes (Table 2) was carried out through spectrometric measurements at their respective absorption peaks and molar extinction coefficients (ε). Mn(III)-DFOB has a characteristic dark green color with an absorption peak at 640 nm ($\varepsilon = 1.09 \times 10^2$ mol^{-1} L cm^{-1}; Beyer Jr. and Fridovich (1989)), but, for quantification, we used a shoulder (310-320 nm) of the absorbance spectra in the UV range, at 310 nm $\varepsilon = 2.055 \times 10^3$ mol^{-1} L cm^{-1}; Duckworth and Sposito (2005).

2.5.1 Recovery of Mn(III)-L by DFOB

Ligand exchange reactions are time and concentration dependent. Knowing rates of the metal exchange between ligands will ensure that the reaction has been completed within a given period of time. Precise rates of manganese(III) ligand-exchange to DFOB from 4.2 mM manganese(III)-pyrophosphate, 3.0 mM manganese(III)-pyruvate, 2.9 mM manganese(III)-malonate, and 4.8 mM manganese(III)-citrate could not be determined as the formation of the Mn(III)-DFOB occurred within 8 s, approximately the time required by a SpectraMax M2 to complete a full scan (200 to 800 nm, 4 nm resolution). Rapid Mn(III)-DFOB formation, consistent with the work of Trouwborst et al. (2006), occurred in experiments where DFOB was added at five-times the concentration of the aforementioned Mn(III)-L complexes in 20 mM pH 7.8 HEPES (data not shown). Rapid Mn(III)-DFOB formation also occurred when 10 mL of the stock Mn(III)-L complexes, mentioned above, were added to 100 mL of aged, 0.2 μm filtered, North Atlantic seawater, at an initial S_p of 35 (Fig. 4). A manganese(II) in seawater control was prepared by addition of 10 mL 4.7 mM $MnCl_2$ to 100 mL of seawater. The absorbance of this solution upon the addition of DFOB was monitored at 310 nm over a 30-minute period and no change was detected. This result was expected as the reaction of manganese(II) with DFOB in seawater is negligible due to side reactions of DFOB with Mg^{2+} and Ca^{2+} (Wuttig et al., 2013). Assuming a two-fold increase in the half-life of the dissociation reaction of the Mn(III)-L complex with each 10 °C decrease in temperature (Luther et al., 2015), we estimated that manganese(III) in seawater would conservatively take 1 to 2 minutes to complex with DFOB at 3 °C. As no detectable Mn(III)-DFOB formed from the $MnCl_2$ control solution over 30 minutes, and if we assume that the reaction of manganese(II) with DFOB would follow a similar temperature dependence to the dissociation of the Mn(III)-L complex, there should be no interference from manganese(II) within 2 hours.

2.5.2 Extraction of Mn(III)-L_{DFOB}

Extraction of newly synthesized Mn(III)-DFOB from DI by the HLB cartridges can be up to 100 % effective (Fig. 5). To ascertain whether once run dry (manufacturer's notes), the Oasis HLB cartridges could be reused and how stable they were at recovering Mn(III)-DFOB, comparisons were made between new and used (approximately 50 times) 225 mg cartridges.

Recovery experiments used a Mn(III)-DFOB solution that had undergone some decomposition; 383 μM Mn(III)-DFOB solution with a total manganese concentration of 546 ± 12 μM, as measured using formaldoxime (Brewer and Spencer, 1971). Mn(III)-DFOB, quantifiable by its shoulder at 310 nm, was only present in the first methanol eluate. New cartridges recovered 351 ± 11 μM (n = 4) or 92 ± 3 % of the sample whereas used cartridges recovered 357 ± 23 μM (n = 4) or 93 ± 6 % of the sample.

Mn(III)-DFOB was also extracted from the seawater ligand exchange experiments (Section 2.5.1, Fig. 4). Sample effluents, following ligand exchange from Mn(III)-pyruvate, -citrate and -malonate and the HEPES wash (Fig. 6), produced absorbance spectra in the UV range when in seawater. These spectra were not of Mn(III)-DFOB (no characteristic shoulder beginning at 310 nm (location indicated by red lines, Fig. 6)), but of the seawater plus residual ligand or HEPES. The methanol eluates showed characteristic Mn(III)-DFOB spectra in the UV region (Fig. 6). To ascertain, that in these eluates, the visible green color was Mn(III)-DFOB, the absorbance peak at 640 nm was also measured. Following elution, the cartridges had recovered 93 to 100 % of the Mn(III)-DFOB from the seawater (Table 3).

Though Mn(III)-DFOB in methanol can be measured by both analytical techniques, FIA-S and ICP-MS (Section 2.5.4), to limit any potential differences due to using a manganese(II) standard, the Mn(III)-DFOB was reduced to manganese(II). The strong reducing agent, NH_2OH-HCl, was added prior to acidification of the sample. In addition to NH_2OH-HCl directly reducing Mn(III)-DFOB to manganese(II), the decrease in pH through acidification would also have induced the decomposition of Mn(III)-DFOB by intramolecular electron transfer resulting in manganese(II) and oxidized DFOB. However, different forms of oxidized DFOB can form stable complexes with manganese(II) and at an alkaline pH, the manganese(II) in these complexes can undergo air-oxidation to manganese(III) (Duckworth and Sposito, 2005). In addition to the DFOB oxidation products, there are unknown organics eluting from the OASIS HLB cartridges (Section 2.5.4), these may also form complexes with the manganese following its air oxidation from manganese(II) to manganese(III). The addition of the reducing agent inhibits the air oxidation of manganese(II) during the buffering of the samples to pH 8.8 prior to FIA-S analysis.

2.5.3 Mn(III)-DFOB field sample processing

To induce manganese(III) ligand exchange in field samples, small volume aliquots of 12.8 mM DFOB (< 120 hours old) were added to each 50 mL of filtrate, to a final concentration of 56.1 μM. This final concentration of DFOB is ~3× the concentration (20 μM) used during the electrochemical detection of Mn(III)-DFOB in Black Sea off-shore waters (Trouwborst et al., 2006), the higher final concentration ensured a competitive edge against the likely increase in concentration of the natural organic material/ligand pool expected in estuarine and coastal systems. Samples were shaken and left to react for 45 minutes. Prior to extraction of Mn(III)-DFOB, the HLB cartridges were washed and primed. The reagents required and order in which they were used for initializing the cartridges and extracting the Mn(III)-DFOB are presented in Fig. 2. Extractions on every 10th sample were performed in triplicate, and triplicate blanks were taken for every 10 samples extracted. The blank for Mn(III)-DFOB was 0.2 μm filtered DI pumped through the HLB cartridges followed by elution with methanol. Samples and blanks in methanol were supplemented by small volumes of 1 % NH_2OH-HCl to a final concentration of 144 μM. These were sealed and, on return to the laboratory, stored at -20 ˚C to avoid evaporation. To ensure samples were at a similar pH to standards, after two further weeks, 2 μL of 6 M HNO_3 were added per 1 mL of sample before they were again placed at -20˚C.

2.5.4 Quantification of Mn(III)-L_{DFOB} in methanol by FIA-S

The Mn(III)-DFOB samples in methanol were measured by Tiron FIA-S (Fig. 3); a description of the protocol for FIA-S analysis which extracts manganese from the methanol sample using the Toyopearl AF-Chelate-650M is provided in Fig. 2. In the presence of H_2O_2, manganese catalyzes the oxidation of the sulfonated catechol Tiron to its semiquinone form (Scharff and Genin, 1975). The semiquinone complex formed at pH>9 has an absorbance band at 424 nm and serves to quantitatively determine total dissolved manganese spectrophotometrically (Chaparro et al., 2016; Lewis and Luther, 2000; Mallini and Shiller, 1993; Otto et al., 1983). In a 100-cm LWCC, the direct measurement of the Tiron semiquinone complex is affected by the absorbance of methanol. Therefore, to isolate the Mn(III)-DFOB from methanol, an AF-Chelate-650M stationary phase chromatography column was used. This stationary phase has been used to concentrate low concentrations of metals (Milne et al., 2010) including manganese (Aguilar-Islas et al., 2006) from seawater. The method was verified for manganese on a 10-fold dilution of the National Research Council Canada SLEW-3 certified reference material (S_p ~33 and dMn_T =

29.5 ± 4 nM); the dilution is comparable to samples used for ICP-MS measurements (Section 2.4.2). Replicate analyses using the FIA-S yielded total manganese concentrations of 29.4 and 30.0 nM.

The sensitivity of a 100-cm LWCC requires that there is a prior knowledge of optimal reagent concentrations to provide the most precise analytical range. This ensures that the highest signal to noise ratio is obtained, and it improves measurement accuracy through placing a sample's signal centrally within a calibration curve (Miller and Miller, 1993). In a 100-cm cell, the analytical ranges for the following concentrations of Tiron, 0.5, 1.0, 3.2 and 6 mM, are, 0-300, 0-60, 0-10 and 0-4 nM, respectively. As the analytical range decreases, the limit of detection, based on the standard deviation of four blanks, also decreases. The achievable limits of detection upon loading 1 mL of $MnSO_4$ standard in methanol on to AF-Chelate-650M, 18 μL columns, are 4.3 nM (0.5 mM Tiron), 0.31 nM (1.0 mM Tiron), 0.06 nM (3.2 mM Tiron) and 0.01 nM (6 mM Tiron). Concentrations of Mn(III)-L_{DFOB} derived from the St. Lawrence Estuary samples were unknown; therefore, each sample was pre-measured, some twice (surface transect) to provide a semi-quantitative analysis and allow a match with a suitable calibration range. Samples were measured using 0.5 or 1.0 mM Tiron. As samples were concentrated through the OASIS HLB cartridges, the limits of detection, corrected for the concentration factor (50 mL to 3.5 mL), at the time of measurement of the samples were 0.5 nM (0.5 mM Tiron) and 0.09 nM (1.0 mM Tiron). Samples from Station SAG30, Station 23 and Station 17 were also analyzed by ICP-MS. The need to use aliquots of the samples for semi-quantitative analysis and for ICP-MS limited us to only duplicate measurements for final quantification by FIA-S. The average error of these measurements was 4 ± 3 %, compared to the average for standards which was 0.6 %.

Samples in methanol measured using ICP-MS (Fig. 7) required a 10-fold dilution with 1 % HNO_3. Dilution resulted in a flocculation of dissolved acidic-polysaccharides which had co-eluted from the samples with the Mn(III)-DFOB. The presence of acidic-polysaccharides was confirmed using the Alcian blue test (Passow and Alldredge, 1995), as the salt interference on the test was avoided through the Mn(III)-DFOB extraction protocol. Within 24-h, all visible flocculates had migrated to the surface of the sample. The samples were left to stand for between 72-100 h before 4 mL of solution was removed from below the polysaccharide layer and filtered through a 0.2 μm membrane prior to ICP-MS analysis. The slope of the linear correlation

(coefficient of determination, $r^2 = 0.89$) between measurements, FIA-S and ICP-MS, was 0.92 (Fig. 7), indicating that Tiron FIA-S measures approximately 92 % of the ICP-MS concentration. Though recoveries were not 100 %, for low and sub-nanomolar concentrations, the recovery is reasonable. For comparison, the data sheet of the certified reference material SLEW-3, states an error of ±14 % for its manganese concentration.

3.0 Results

The Saguenay Fjord water column is well oxygenated, although the oxygen concentration decreases from ~300 to 230 μM from surface to bottom. The Saguenay Fjord surface water transect (Table 4, Fig. 8) consisted of waters within a salinity range of 13.2 ± 1.5. The sample at Station SAG05 within this salinity range was collected at a depth of 5 m ($S_P = 14.3$). Throughout the surface transect, dMn_T was invariant, 55 ± 1.3 nM, MnO_2 decreased from 7.5 nM at SAG05 to 1.3 nM at SAG48 and, in contrast, Mn(III)-L_{DFOB} generally increased from 0.5 nM at SAG05 up to 8 nM at SAG42. The dMn_T concentrations within the top 10 m of the water columns at SAG05 and SAG30 were similar (Table 4, Fig. 9): At SAG05, dMn_T decreased from 56 nM (5 m; $S_P = 14.3$) to 34 nM (10 m; $S_P = 26.4$) and at SAG30 from 54 nM (3 m; $S_P = 15.0$) to 39 nM (10 m; $S_P = 24.8$). The full dMn_T vertical profiles at SAG05 displayed a mid-depth minimum (34 nM; 10 m, $S_P = 26.4$) and concentrations increased linearly with depth to the bottom (180 nM; $S_P = 29.4$). At SAG30, the dMn_T minimum (21 nM) occurred deeper in the water column (50 m; $S_P = 29.1$) and dMn_T remained lower in the mid-depths until a sharp increase between 150-200 m to a maximum in the bottom water (490 nM; $S_P = 30.8$). The dMn_T increase with depth is likely indicative of dMn_T fluxing out of the sediments. Mn(III)-L_{DFOB} (Table 4, Fig. 9) was generally low at SAG05, up to 1.8 nM was present at 60 m ($S_P = 29.1$), but concentrations decreased sharply to 0.4 nM in the bottom water (85 m; $S_P = 29.4$), while MnO_2, between 10 m and the bottom, was generally constant, on average 11 ± 1.5 nM. At SAG30, the concentrations of MnO_2 and Mn(III)-L_{DFOB} between 20 and 150 m remained invariant, 2.6 ± 0.1 nM and 16 ± 2 nM, respectively. In the deepest waters (200-250 m), Mn(III)-L_{DFOB} increased to an average of 3.9 ± 0.1 nM while MnO_2 increased to a maximum of 22 nM at 200 m, and then decreased to 13 nM in the bottom water.

In the Laurentian Channel, the seaward flowing surface waters at Stations 23 and 17, contained 4.2 and 1.6 nM MnO_2 and 2.0 and 2.2 nM Mn(III)-L_{DFOB} at S_p of 27.8 and 29.9, respectively (Fig. 10). When the concentrations of MnO_2 and Mn(III)-L_{DFOB} in the surface waters are integrated over the depth of the pycnocline (20 m), total MnO_2 decreases seaward from 11 ± 7 to 2.3 ± 0.3 nM while Mn(III)-L_{DFOB} increases from 1.4 ± 0.7 to 1.7 ± 0.6. In contrast, in the core of the CIL (90 m rising to 60-80 m; S_P = 32.2), which moves landward along the Laurentian Channel between Stations 17 and 23, MnO_2 increases from 2.9 ± 0.6 to 10 ± 1.0 nM while Mn(III)-L_{DFOB} increases, albeit less significantly, from 0.9 ± 0.1 to 1.4 ± 0.1.

At Station 17 (Fig. 9), oxygen concentrations were high in the CIL (302 ± 50 μM) while MnO_2 concentrations were low (2.3 ± 1.0 nM). In contrast, deep waters (σ_θ = 27.5-28; S_P = 34.3-34.8) had low oxygen concentrations, which increased with depth (114 to 141 μM; 35 % oxygen saturation increasing to 44 %) between 250 and 390 m, while MnO_2 increased concomitantly five-fold from 10 to 52 nM. The most significant change in MnO_2 concentration was recorded in the deep waters (σ_θ = 27-27.2; S_P = 34.3-34.5) at Station 23 (Fig. 9, Table 4), where the dissolved oxygen concentrations were lowest, decreasing with depth from 83 to 55 μM (26 % oxygen saturation decreasing to 17 %) between 200 and 340 m, while MnO_2 increased from 170 to 1070 nM. For both St. Lawrence Estuary stations, between the core of the CIL and into the deep water, Mn(III)-L_{DFOB} was relatively invariant, 0.8 ± 0.1 nM (Station 17, 60 – 350 m) and 0.9 ± 0.1 nM (Station 23, 50 – 250 m). The highest Mn(III)-L_{DFOB} concentration, 2.7 nM, was measured at 300 m depth (σ_θ = 27.21; S_P = 34.5) at Station 23 with the concentration decreasing to 1.9 nM in the bottom water at 340 m (σ_θ = 27.22; S_P = 34.5).

4.0 Discussion

4.1 Mn(III)-DFOB

The quantitative recovery of Mn(III)-DFOB in the methanol eluate demonstrates that DFOB outcompetes weaker ligands (log K_{COND} < 13.2 (Luther et al., 2015)), such as pyrophosphate in freshwater (Trouwborst et al., 2006), environmental ligands in suboxic seawaters (Madison et al., 2011; Trouwborst et al., 2006) and pyruvate, malonate and citrate in seawater, for manganese(III). When combined with the use of solid phase extraction columns, the method allows for the concentration, recovery and detection of weakly complexed manganese(III) in

natural waters. Previous analytical methods to determine manganese(III) in marine waters used either an electrochemical approach with DFOB as the competitive ligand (Trouwborst et al., 2006) or the porphyrin spectrophotometric method (Madison et al., 2011). The limit of detection of the DFOB extraction method described and used in this work, 0.09 nM, is lower than that of the electrochemical approach without a chromatographic pre-concentration, on the order of 150 nM in seawater. It is also lower relative to the porphyrin spectrophotometric method (3 nM), though the porphyrin method utilizes various protocols with which to measure different fractions of the soluble manganese pool. The first variant can distinguish between manganese(II) and weak Mn(III)-L complexes (detection limit for speciation in seawater, 300 nM (Madison et al., 2011)). The second variant measures two fractions, to a detection limit of 3 nM. These fractions are, manganese(II) plus weak Mn(III)-L complexes and the total soluble manganese; strong Mn(III)-L complexes are determined by the difference between measurements prior to and after reduction at 90 ˚C in the presence of hydroxylamine (Oldham et al., 2017b).

In seawater, the air oxidation of manganese(II) complexed with DFOB can form Mn(III)-DFOB and is dependent on the precursor $MnHDFOB^0$ (rate = $k[MnHDFOB^0][O_2]$: pH_{NBS} 7.6, 0.029 ± 0.003 M^{-1} s^{-1}; pH_{NBS} 7.9, 0.15 ± 0.2 M^{-1} s^{-1}) (Duckworth and Sposito, 2005). Air oxidation is pH dependent and the precursor formation is inhibited by side reactions of DFOB with Mg^{2+} and Ca^{2+}. Only with an addition of >200 μM DFOB to seawater at >pH_{NBS} 8.2, does oxidation of manganese(II) upon exposure to ambient air become significant (Wuttig et al., 2013). In seawater at pH_{NBS} 7.8, and following an addition of 200 μM DFOB (~300× more Mg^{2+} plus Ca^{2+} than DFOB), only 1 % of the manganese(II) is in the form $MnHDFOB^0$ (Wuttig et al., 2013). In the lowest salinity sample, taken from the Saguenay Fjord (S_P = 3.5), there is a total of 6.4 mM Mg^{2+} plus Ca^{2+} based on conservative mixing between the river end member, taken as average concentrations in the Saguenay River (0.021 mM Mg^{2+} and 0.050 mM Ca^{2+} (Millot et al., 2002)) and seawater (52.8 mM Mg^{2+} and 10.3 mM Ca^{2+}). This concentration, though significantly lower than undiluted seawater, is still 120× higher than the final DFOB concentration. The resulting ratio of DFOB to Mg^{2+} plus Ca^{2+} is still ~50 % lower than the upper limit required for a significant effect, as suggested by Wuttig et al. (2013). If we assume that the effect of Mg^{2+} plus Ca^{2+}on DFOB complexation of manganese(II) is limited in proportion to their lower concentrations, it is likely to be ~50 % lower at Sp = 3.5 with 56 μM DFOB resulting in an increase to 5 % of the manganese(II) present as $MnHDFOB^0$. Incorporating a temperature

453 correction (Luther et al., 2015), after 68 minutes (average time from the first to last milliliter of
454 sample extracted), the oxidation by ambient air of 50 nM manganese(II) (~2.5 nM $MnHDFOB^0$
455 at $S_p = 3.5$) would form between 0.12 (pH_{NBS} 7.8) and 0.19 nM (pH_{NBS} 7.9) Mn(III)-DFOB
456 (Duckworth and Sposito, 2005). In the Saguenay Fjord at station SAG05, samples were taken at
457 depths of 2 (0.9 nM Mn(III)-L; $S_p = 3.5$, pH_T (total proton scale) 7.72/pH_{NBS} 7.87) and 5 m (0.5
458 nM Mn(III)-L; $S_p = 14.3$, pH_T 7.78/pH_{NBS} 7.93). In the shallower sample, it is possible that up to
459 20 % of the Mn(III)-DFOB was sourced from ambient air oxidation of Mn(II)-DFOB and not
460 formed from the competitive equilibration of manganese(III) natural ligand complexes. Though
461 this potential interference has significance in terms of the Mn(III)-L_{DFOB} concentration, its
462 relative contribution within the total concentration of all manganese species measured in that
463 sample is insignificant (<0.3 %). In the lower sample, at $S_p = 14.3$, there was 470× more Mg^{2+}
464 and Ca^{2+} than DFOB, so it is unlikely that there was an effect.

465 Mn(III)-DFOB will form from the reductive dissolution of MnO_2 but, even though nano-MnO_2
466 may be found in organic(lignin)-rich freshwater environments (Krachler et al., 2012) and enzyme
467 preparations in the laboratory (Romano et al., 2017), it is highly unlikely that nano- or colloidal-
468 MnO_2 is present in the 0.2 μm filtrate. On formation, nano/colloidal-MnO_2 has a negative
469 electrostatic charge. The presence of cations neutralizes this charge, inducing the nano/colloidal-
470 MnO_2 to rapidly coagulate and precipitate (Perez-Benito et al., 1989). Divalent ions are better
471 coagulating agents than monovalent ones (Perez-Benito et al., 1989), which is why the presence
472 of Mg^{2+} and Ca^{2+} in river, estuarine and seawater inhibits the presence of nano-/colloidal MnO_2.
473 Even in the presence of colloidal MnO_2, when stabilized in an organic rich-environment, these
474 colloids are vulnerable to loss through flocculation as the ionic strength increases (Krachler et
475 al., 2012). In addition, as free enzyme concentrations in environmental systems are typically very
476 low this direct formation mechanism is limited. Typically, the enzymatic formation of MnO_2
477 occurs on biological surfaces, which are larger than the filtrate cut-off, and while the accretion of
478 manganese oxides is enhanced at surfaces (Morgan, 2000), particulate material is also unlikely to
479 pass through the 0.2 μm membrane.

480 In the St. Lawrence Estuary and Saguenay Fjord, strong ($\log K_{COND} > 13.2$) Mn(III)-L complexes
481 are believed to be predominantly humic-type complexes (Oldham et al., 2017b) and likely not
482 readily available to (bio)degradation (Wright et al., 2018). The formation of these complexes is

attributed to humic chelation following manganese(II) oxidation and they were found to be present over a concentration range from 6 to 480 nM (Oldham et al., 2017b). The disparity in the recovery of manganese(III) between the porphyrin technique (with added reductant) and the DFOB technique indicates that DFOB is not outcompeting the stronger humic-like complexes. Terrestrial humic material appears to behave conservatively in the Saguenay Fjord waters (Xie et al., 2012). Nevertheless, since neither Mn(III)-L_{DFOB} nor MnO_2 display conservative mixing in the surface water transect, the ubiquitous presence of natural ligands that bind manganese(III) and react with DFOB to form Mn(III)-L_{DFOB} suggests that both terrestrial and marine ligands may be integral in manganese(III) stabilization. Furthermore, as Mn(III)-L_{DFOB} was found in samples at all locations and depths, the organic ligand(s) may be produced *in situ*, ligands such as microbially-produced siderophores or organic matter degradation metabolites. Siderophores come in two major classes depending on the ligating moieties, hydroxamates and catecholates (Johnstone and Nolan, 2015). The majority of strong iron(III) siderophores use catecholate moieties though there are also other groups of strong siderophores, for example α-hydroxyaspartic acids (Hider and Kong, 2010; Hardy and Butler, 2018). Theoretically, Mn(III)-catecholate complexes are not as likely to form in the environment due to the short `bite distance' of catecholate oxygen atoms (2.79 Å) which are unable to span the elongated coordination axes of the Jahn-Teller distorted manganese(III) (Sheriff et al., 2004). Though high, the stability of the Mn(III)-DFOB complex (log $K_{[Mn(III)HDFOB+]}$ = 28.6 ± 0.5 in 0.1 M NaCl (Duckworth and Sposito, 2005), log K_{COND} = 13.2 (Luther et al., 2015)) is less than with some siderophores, such as the mixed catecholate hydroxamate siderophore, pyoverdine (Parker et al., 2004). Therefore, even in the presence of excess DFOB, some manganese(III) may be complexed to siderophores that cannot be outcompeted by DFOB.

Mn(III)-L complexes that can be outcompeted by DFOB have only been measured at the sub-oxic interfaces of the Black Sea (0.15 to 4.5 μM) and Chesapeake Bay (up to 2.0 μM) (Trouwborst et al., 2006). Moreover, no weakly complexed manganese(III) has been found in waters with a salinity >30 unless they were anoxic interstitial sediment porewaters (Madison et al., 2013, 2011). Weak Mn(III)-L complexes, measured by the porphyrin technique, have been found in significant concentrations (range 0.4 - 5.6 μM) in a humic-rich estuary (Oldham et al., 2017a). They are also present in the sediment porewaters of the greater St. Lawrence Estuary

513 (Madison et al., 2013), and were recently found to account for up to 20 % of dMn_T in organic-
514 rich waters entering a water treatment plant (Johnson et al., 2018).

515 Throughout the surface transect of the Saguenay Fjord, from SAG05 to SAG48, Mn(III)-L_{DFOB}
516 appears to form via MnO_2 reduction; Mn(III)-L_{DFOB} increases (0.5 up to 6 nM) as MnO_2
517 decreases (8 down to 1 nM). At the same time, dMn_T is generally invariant along this transect. In
518 contrast, no pathways of formation linking Mn(III)-L_{DFOB} and MnO_2 are apparent within the
519 water column of either the Saguenay Fjord or St. Laurence Estuary. There is, however, a
520 similarity in their distribution at mid-depths (20-150 m) at SAG30, where both Mn(III)-L_{DFOB}
521 and MnO_2 concentrations are invariant, (2.7 ± 0.1 and 16 ± 2 nM). The differences in the rates of
522 removal, diffusion combined with advection and mixing versus precipitation, should result in a
523 progressive decrease of the particulate concentration with depth. As there is no loss of MnO_2
524 over this depth range (> half of the water column) there is likely production of MnO_2 as a
525 balance to precipitation. Mn(III)-L_{DFOB} is more favorably oxidized to MnO_2 than strong Mn(III)-
526 L complexes (Wright et al., 2018) so, for Mn(III)-L_{DFOB} to also remain invariant, *in situ*
527 production is required. In the same waters at SAG30, strongly complexed manganese(III) varied
528 moderately (32 ± 11 nM), while the concentration of manganese(II) + Mn(III)-L_{weak} reported in
529 Oldham et al. (2017b), showed a significant increase from 40 (20-50 m) up to 150 ± 14 nM (100-
530 150 m). At this location, the pool of manganese that presents the greatest concentration change is
531 the manganese(II) + Mn(III)-L_{weak} pool, but within this pool Mn(III)-L_{DFOB} ≈ Mn(III)-L_{weak} was
532 invariant.

533 ### 4.2 MnO_2

534 In the St. Lawrence Estuary, below the core of the CIL, MnO_2 concentrations increase with
535 depth. Sources of MnO_2 to the water column are typically *in-situ* oxidation of manganese(II) and
536 manganese(III), and detrital input, as evidenced by the reversed gradient of MnO_2 between
537 surface waters and the core of the CIL (Fig. 10). Concentrations of MnO_2 were low in the CIL at
538 Station 17 likely due to the formation of these waters during winter in the Gulf of the St.
539 Lawrence, a location where there is significant ice cover (Government of Canada, 2010) and
540 detrital material is probably mostly supplied by aeolian deposition. Microbial manganese
541 oxidation is an oxygen-dependent surface-catalyzed process (Clement et al., 2009), therefore,
542 increasing concentrations of MnO_2 with depth might be expected to show some relationship to

543 the concentration of dissolved oxygen. As deep waters of the St Lawrence Estuary move
544 landward, their oxygen level decreases from 40 to less than 20 % saturation leading to an inverse
545 relationship between dissolved oxygen and MnO_2. Though biologically-catalyzed manganese(II)
546 oxidation at low (<3 μM O_2) oxygen concentrations can occur, its rate is slower than at higher
547 oxygen levels (Clement et al., 2009; Tebo and Emerson, 1985). Rates of apparent oxidation in
548 these waters were high enough for MnO_2 to accumulate, as revealed by the relative increase of
549 MnO_2 between Stations 17 and 23. Integrating the MnO_2 concentrations of the deep waters
550 [Station 17, σ_θ = 27.5-28.2; Station 23, σ_θ = 27-27.2 (highlighted in bold in Table 4)], the MnO_2
551 content increased approximately 20-fold (52 up to 1070 nM in the bottom waters). This is in
552 stark contrast to the Saguenay Fjord where MnO_2 concentrations were lower (16 ± 3 nM between
553 20 and 250 m) under high oxygen conditions. The increase in MnO_2 in the Gulf and Lower St.
554 Lawrence Estuary corresponds to the approximate difference in the flux of soluble manganese
555 out of the sediments to the overlying water column between the two stations. At Station 17, the
556 flux is barely detectable (<1 μmol cm^{-2} yr^{-1}) whereas it is between 11 (Sundby and Silverberg,
557 1985) and 17 (Lefort, 2011) μmol cm^{-2} yr^{-1} at Station 23. The rate of formation of MnO_2 is
558 dependent on the concentration of both manganese(II) and oxygen, the sharp increase of MnO_2
559 with depth in the deep waters of the St. Lawrence Estuary is likely due to a chain of processes.
560 Soluble manganese escapes these sediments (Madison et al., 2013; Oldham et al., 2017b; Sundby
561 and Silverberg, 1985), through biological activity (Richard et al., 2013), into the overlying water
562 which has oxygen concentrations at under 40 % saturation. The MnO_2 then forms, most likely
563 through microbially catalyzed oxidation (Sunda and Huntsman, 1988, 1987; Tebo and Emerson,
564 1986). To allow the accumulation of particulate manganese, either the rate of the final production
565 stage of these processes has increased, because of the increasing soluble manganese
566 concentration and decreasing dissolved O_2 concentration or the water column removal
567 mechanism for MnO_2 decreased. The landward increase in particulate manganese concentrations
568 in the bottom waters of the St. Lawrence Estuary was documented five decades ago and was
569 believed to comprise two primary components, *in-situ* production combined with re-suspension
570 of very fine-grained material (Sundby, 1977; Sundby et al., 1981). The addition of winnowing to
571 *in-situ* production was coined the *broom affect* (Sundby et al., 1981). The mechanisms behind
572 the accumulation of MnO_2 in the main estuary did not appear to affect the concentration of
573 Mn(III)-L_{DFOB}, which remained low. In contrast, the Mn(III)-L_{DFOB} concentrations in the

574 Saguenay Fjord at SAG30 were higher in the presence of lower MnO_2 and higher oxygen
575 concentrations.

576 **5.0 Conclusion**

577 Previous work has shown that dissolved manganese(III) complexes (Mn(III)-L) can be divided
578 into two classes, weak and strong as denoted by their ability to either react with the cadmium
579 substituted porphyrin in a competition reaction or react as manganese(II) directly after reduction
580 (Luther et al., 2015; Madison et al., 2011; Oldham et al., 2017b, 2017a, 2015). We developed a
581 technique, based on a ligand competition with DFOB, to measure weak Mn(III)-L at very low
582 concentrations in filtered samples, a technique that should be applicable to many oceanic
583 environments. Lower limits of detection are achievable using FIA-S relative to ICP-MS, making
584 FIA-S the likely choice for the measurement of low manganese(III) concentrations found in most
585 oceanic waters. The FIA-S system is also portable and can potentially be used for continuous
586 flow analysis. Although we do not know what comprises the weak ligands, they can include
587 many siderophores and likely carboxylate-rich organic matter degradation products. Using this
588 technique, we show that this weaker class of natural ligands, that bind manganese(III) and react
589 with DFOB to form Mn(III)-L_{DFOB} complexes, is ubiquitous throughout the greater St. Lawrence
590 Estuary, albeit at low nanomolar concentrations. These weak complexes account for a minor
591 fraction of the total Mn(III)-L in this location, relative to those that were previously measured
592 (Oldham et al., 2017b), indicating that the predominant Mn(III)-L complexes in the St. Lawrence
593 Estuary are formed with strong ligands, such as humics. Attributing a mechanism of Mn(III)-
594 L_{DFOB} formation remains elusive and the low concentrations of this soluble manganese(III) pool
595 are paradoxical, although siderophore type ligands are normally low in concentration compared
596 to humic material and other organic matter decomposition products (Mawji et al., 2008). Low
597 concentrations may indicate that this pool is reactive and more susceptible to oxidation and
598 reduction than strong ligand complexes. However, the ubiquitous presence of Mn(III)-L_{DFOB}
599 suggests they either possess a degree of stability or that there is a dynamic production and
600 removal system in near-equilibrium: Either Mn(III)-L_{DFOB} characteristic could support the theory
601 (Johnson, 2006) that deep oceanic dissolved manganese is made up of significant quantities of
602 Mn(III)-L. Accordingly, we propose that this operationally-defined Mn(III)-L pool is likely an
603 important player in coupled reactions with other biogeochemical cycles. The development of the

new low-level DFOB extraction technique, in combination with traditional (total dissolved) and specific MnO_2 (rather than a particulate manganese) measurements, may provide new insights into processes involved in the production and consumption of manganese(III) and help unravel the complexity of the environmental manganese cycle.

Acknowledgments

This work was funded by grants from the Chemical Oceanography program of the National Science Foundation (OCE-1558738 and OCE-1155385 to GWL; OCE-1558692 and OCE-1154307 to BMT) and the National Sciences and Engineering Research Council of Canada (NSERC) through Discovery and Ship-time grants to AM. We are also grateful to the captain and crew of the R/V *Coriolis II* for their hospitality as well as Gilles Desmeules for his help in acquiring water and sediment samples for this research.

616 Bibliography

617

618 Aguilar-Islas, A.M., Resing, J.A., Bruland, K.W., 2006. Catalytically enhanced
619 spectrophotometric determination of manganese in seawater by flow-injection
620 analysis with a commercially available resin for on-line preconcentration.
621 Limnology and Oceanography: Methods 4, 105–113.
622 https://doi.org/10.4319/lom.2006.4.105
623 Archibald, F.S., Fridovich, I., 1982. The scavenging of superoxide radical by manganous
624 complexes: In vitro. Archives of Biochemistry and Biophysics 214, 452–463.
625 https://doi.org/10.1016/0003-9861(82)90049-2
626 Barbeau, K., Rue, E.L., Trick, C.G., Bruland, K.T., Butler, A., 2003. Photochemical
627 reactivity of siderophores produced by marine heterotrophic bacteria and
628 cyanobacteria based on characteristic Fe(III) binding groups. Limnology and
629 Oceanogrography 48, 1069–1078.
630 Bargar, J.R., Tebo, B.M., Bergmann, U., Webb, S.M., Glatzel, P., Villalobos, M., 2005.
631 Biotic and abiotic products of Mn(II) oxidation by spores of the marine Bacillus
632 sp. strain SG-1. American Mineralogist 90, 144–154.
633 Belzile, M., Galbraith, P.S., Bourgault, D., 2016. Water renewals in the Saguenay Fjord.
634 J. Geophys. Res. Oceans 121, 638–657. https://doi.org/10.1002/2015JC011085
635 Beyer Jr., W.F., Fridovich, I., 1989. Characterization of a superoxide dismutase mimic
636 prepared from desferrioxamine and MnO_2. Archives of Biochemistry and
637 Biophysics 271, 149–156. https://doi.org/10.1016/0003-9861(89)90265-8
638 Brewer, P.G., Spencer, D.W., 1971. Colorimetric determination of manganese in anoxic
639 water. Limnology and Oceanography 16, 107–112.
640 Chaparro, L., Ferrer, L., Leal, L.O., Cerdà, V., 2016. Automatic flow analysis method to
641 determine traces of Mn^{2+} in sea and drinking waters by a kinetic catalytic process
642 using LWCC-spectrophotometric detection. Talanta 148, 583–588.
643 https://doi.org/10.1016/j.talanta.2015.10.050
644 Clement, B.G., Luther, G.W., Tebo, B.M., 2009. Rapid, oxygen-dependent microbial
645 Mn(II) oxidation kinetics at sub-micromolar oxygen concentrations in the Black
646 Sea suboxic zone. Geochimica et Cosmochimica Acta 73, 1878–1889.
647 https://doi.org/10.1016/j.gca.2008.12.023
648 Dellwig, O., Schnetger, B., Brumsack, H.-J., Grossart, H.-P., Umlauf, L., 2012.
649 Dissolved reactive manganese at pelagic redoxclines (part II): Hydrodynamic
650 conditions for accumulation. Journal of Marine Systems 90, 31–41.
651 https://doi.org/10.1016/j.jmarsys.2011.08.007
652 Duckworth, O.W., Sposito, G., 2005. Siderophore−manganese(III) interactions. I. Air-
653 oxidation of manganese(II) promoted by Desferrioxamine B. Environ. Sci.
654 Technol. 39, 6037–6044. https://doi.org/10.1021/es050275k
655 Duke, F.R., 1947. The theory and kinetics of specific oxidation. I. The trivalent
656 manganese-oxalate reaction. J. Am. Chem. Soc. 69, 2885–2888.
657 https://doi.org/10.1021/ja01203a073

Faulkner, K.M., Stevens, R.D., Fridovich, I., 1994. Characterization of Mn(III) complexes of linear and cyclic desferrioxamines as mimics of superoxide dismutase activity. Archives of Biochemistry and Biophysics 310, 341–346. https://doi.org/10.1006/abbi.1994.1176

Glenn, J.K., Akileswaran, L., Gold, M.H., 1986. Mn(II) oxidation is the principal function of the extracellular Mn-peroxidase from *Phanerochaete chrysosporium*. Archives of Biochemistry and Biophysics 251, 688–696. https://doi.org/10.1016/0003-9861(86)90378-4

Government of Canada, 2010. Sea Ice Climatic Atlas for the East Coast 1981-2010 (program results).

Heintze, S.G., Mann, P.J.G., 1947. Soluble complexes of manganic manganese. The Journal of Agricultural Science 37, 23–26. https://doi.org/10.1017/S0021859600013009

Johnson, K.L., McCann, C.M., Wilkinson, J.-L., Jones, M., Tebo, B.M., West, M., Elgy, C., Clarke, C.E., Gowdy, C., Hudson-Edwards, K.A., 2018. Dissolved Mn(III) in water treatment works: Prevalence and significance. Water Research 140, 181–190. https://doi.org/10.1016/j.watres.2018.04.038

Johnson, K.S., 2006. Manganese redox chemistry revisited. Science 313, 1896–1897. https://doi.org/10.1126/science.1133496

Johnstone, T.C., Nolan, E.M., 2015. Beyond iron: Non-classical biological functions of bacterial siderophores. Dalton Trans 44, 6320–6339. https://doi.org/10.1039/c4dt03559c

Klewicki, J.K., Morgan, J.J., 1999. Dissolution of β-MnOOH particles by ligands: pyrophosphate, ethylenediaminetetraacetate, and citrate. Geochimica et Cosmochimica Acta 63, 3017–3024. https://doi.org/10.1016/S0016-7037(99)00229-X

Klewicki, J.K., Morgan, J.J., 1998. Kinetic behavior of Mn(III) complexes of pyrophosphate, EDTA, and citrate. Environ. Sci. Technol. 32, 2916–2922. https://doi.org/10.1021/es980308e

Kostka, J.E., Luther, G.W., Nealson, K.H., 1995. Chemical and biological reduction of Mn(III)-pyrophosphate complexes: Potential importance of dissolved Mn(III) as an environmental oxidant. Geochimica et Cosmochimica Acta 59, 885–894.

Krachler, R., von der Kammer, F., Jirsa, F., Süphandag, A., Krachler, R.F., Plessl, C., Vogt, M., Keppler, B.K., Hofmann, T., 2012. Nanoscale lignin particles as sources of dissolved iron to the ocean. Global Biogeochem. Cycles 26, GB3024. https://doi.org/10.1029/2012GB004294

Krumbein, W.E., Altmann, H.J., 1973. A new method for the detection and enumeration of manganese oxidizing and reducing microorganisms. Helgolander Wiss. Meeresunters 25, 347–356. https://doi.org/10.1007/BF01611203

Lebel, J., Pelletier, E., Bergeron, M., Belzile, N., Marquis, G., 1983. Le Panache du Saguenay. Can. J. Fish. Aquat. Sci. 40, 52–60. https://doi.org/10.1139/f83-008

Lefort, S., 2011. A multidisciplinary study of hypoxia in the deep water of the Estuary and Gulf of St. Lawrence: Is this ecosystem on borrowed time? (Ph.D). McGill University.

Lewis, B.L., Luther, G.W., 2000. Processes controlling the distribution and cycling of manganese in the oxygen minimum zone of the Arabian Sea. Deep Sea Research Part II: Topical Studies in Oceanography 47, 1541–1561. https://doi.org/10.1016/S0967-0645(99)00153-8

Luther, G.W., Madison, A.S., Mucci, A., Sundby, B., Oldham, V.E., 2015. A kinetic approach to assess the strengths of ligands bound to soluble Mn(III). Marine Chemistry, SCOR WG 139: Organic Ligands – A Key Control on Trace Metal Biogeochemistry in the Ocean 173, 93–99. https://doi.org/10.1016/j.marchem.2014.09.006

Luther, G.W., Ruppel, D.T., Burkhard, C., 1999. Reactivity of dissolved Mn(III) complexes and Mn(IV) species with reductants: Mn redox chemistry without a dissolution step?, in: Mineral-Water Interfacial Reactions, ACS Symposium Series. American Chemical Society, pp. 265–280. https://doi.org/10.1021/bk-1998-0715.ch013

Madison, A.S., Tebo, B.M., Luther, G.W., 2011. Simultaneous determination of soluble manganese(III), manganese(II) and total manganese in natural (pore)waters. Talanta 84, 374–381. https://doi.org/10.1016/j.talanta.2011.01.025

Madison, A.S., Tebo, B.M., Mucci, A., Sundby, B., Luther, G.W., 2013. Abundant porewater Mn(III) is a major component of the sedimentary redox system. Science 341, 875–878. https://doi.org/10.1126/science.1241396

Magliozzo, R.S., Marcinkeviciene, J.A., 1997. The role of Mn(II)-peroxidase activity of mycobacterial catalase-peroxidase in activation of the antibiotic isoniazid. J. Biol. Chem. 272, 8867–8870. https://doi.org/10.1074/jbc.272.14.8867

Mallini, L.J., Shiller, A.M., 1993. Determination of dissolved manganese in seawater by flow injection analysis with colorimetric detection. Limnology and Oceanography 38, 1290–1295.

Mawji, E., Gledhill, M., Milton, J.A., Tarran, G.A., Ussher, S., Thompson, A., Wolff, G.A., Worsfold, P.J., Achterberg, E.P., 2008. Hydroxamate siderophores: Occurrence and importance in the Atlantic Ocean. Environ. Sci. Technol. 42, 8675–8680. https://doi.org/10.1021/es801884r

Miller, J.C., Miller, J.N., 1993. Statistics for Analytical Chemistry. Ellis Horwood PTR Prentice Hall, New York.

Millot, R., Gaillardet, J., Dupré, B., Allègre, C.J., 2002. The global control of silicate weathering rates and the coupling with physical erosion: new insights from rivers of the Canadian Shield. Earth and Planetary Science Letters 196, 83–98. https://doi.org/10.1016/S0012-821X(01)00599-4

Milne, A., Landing, W., Bizimis, M., Morton, P., 2010. Determination of Mn, Fe, Co, Ni, Cu, Zn, Cd and Pb in seawater using high resolution magnetic sector inductively coupled mass spectrometry (HR-ICP-MS). Analytica Chimica Acta 665, 200–207. https://doi.org/10.1016/j.aca.2010.03.027

742 Morgan, J.J., 2000. Manganese in Natural Waters and Earth's Crust: Its Availability to
743 Organisms, in: Sigel, A., Sigel, H. (Eds.), Manganese and Its Role in Biological
744 Processes, Metal Ions in Biological Systems. Marcel Dekker, New York.
745 Mucci, A., Levasseur, M., Gratton, Y., Martias, C., Scarratt, M., Gilbert, D., Tremblay,
746 J.-É., Ferreyra, G., Lansard, B., 2017. Tidally-induced variations of pH at the head
747 of the Laurentian Channel. Can. J. Fish. Aquat. Sci. https://doi.org/10.1139/cjfas-
748 2017-0007
749 Murray, J.W., Balistrieri, L.S., Paul, B., 1984. The oxidation state of manganese in
750 marine sediments and ferromanganese nodules. Geochimica et Cosmochimica
751 Acta 48, 1237–1247. https://doi.org/10.1016/0016-7037(84)90058-9
752 Oldham, V.E., Miller, M.T., Jensen, L.T., Luther, G.W., 2017a. Revisiting Mn and Fe
753 removal in humic rich estuaries. Geochimica et Cosmochimica Acta 209, 267–
754 283. https://doi.org/10.1016/j.gca.2017.04.001
755 Oldham, V.E., Mucci, A., Tebo, B.M., Luther, G.W., 2017b. Soluble Mn(III)–L
756 complexes are abundant in oxygenated waters and stabilized by humic ligands.
757 Geochimica et Cosmochimica Acta 199, 238–246.
758 https://doi.org/10.1016/j.gca.2016.11.043
759 Oldham, V.E., Owings, S.M., Jones, M.R., Tebo, B.M., Luther, G.W., 2015. Evidence for
760 the presence of strong Mn(III)-binding ligands in the water column of the
761 Chesapeake Bay. Marine Chemistry 171, 58–66.
762 https://doi.org/10.1016/j.marchem.2015.02.008
763 Otto, M., Rentsch, J., Werner, G., 1983. Optimized spectrophotometric determination of
764 trace cobalt and manganese by their catalysis of the tiron-hydrogen peroxide
765 reaction. Analytica Chimica Acta 147, 267–275.
766 Parker, D.L., Morita, T., Mozafarzadeh, M.L., Verity, R., McCarthy, J.K., Tebo, B.M.,
767 2007. Inter-relationships of MnO_2 precipitation, siderophore–Mn(III) complex
768 formation, siderophore degradation, and iron limitation in Mn(II)-oxidizing
769 bacterial cultures. Geochimica et Cosmochimica Acta, Physical Chemistry of Soils
770 and Aquifers: A Special Issue in Honor of Garrison Sposito 71, 5672–5683.
771 https://doi.org/10.1016/j.gca.2007.03.042
772 Parker, D.L., Sposito, G., Tebo, B.M., 2004. Manganese(III) binding to a pyoverdine
773 siderophore produced by a manganese(II)-oxidizing bacterium. Geochimica et
774 Cosmochimica Acta 68, 4809–4820. https://doi.org/10.1016/j.gca.2004.05.038
775 Passow, U., Alldredge, A.L., 1995. A dye-binding assay for the spectrophotometric
776 measurement of transparent exopolymer particles (TEP). Limnology and
777 Oceanography 40, 1326–1335. https://doi.org/10.4319/lo.1995.40.7.1326
778 Perez, J., Jeffries, T.W., 1992. Roles of manganese and organic acid chelators in
779 regulating lignin degradation and biosynthesis of peroxidases by *Phanerochaete*
780 *chrysosporium*. Appl. Environ. Microbiol. 58, 2402–2409.
781 Perez-Benito, J.F., Brillas, E., Pouplana, R., 1989. Identification of a soluble form of
782 colloidal manganese(IV). Inorg. Chem. 28, 390–392.
783 https://doi.org/10.1021/ic00302a002

Richard, D., Sundby, B., Mucci, A., 2013. Kinetics of manganese adsorption, desorption, and oxidation in coastal marine sediments. Limnology and Oceanography 58, 987–996. https://doi.org/10.4319/lo.2013.58.3.0987

Romano, C.A., Zhou, M., Song, Y., Wysocki, V.H., Dohnalkova, A.C., Kovarik, L., Paša-Tolić, L., Tebo, B.M., 2017. Biogenic manganese oxide nanoparticle formation by a multimeric multicopper oxidase Mnx. Nature Communications 8, 746. https://doi.org/10.1038/s41467-017-00896-8

Saucier, F.J., Roy, F., Gilbert, D., Pellerin, P., Ritchie, H., 2003. Modeling the formation and circulation processes of water masses and sea ice in the Gulf of St. Lawrence, Canada. J. Geophys. Res. 108, 3269. https://doi.org/10.1029/2000JC000686

Scharff, J.P., Genin, R., 1975. Chélates du manganese(II) avec des coordinats phénoliques: Partie I. Complexes simples binaires. Analytica Chimica Acta 78, 201–209. https://doi.org/10.1016/S0003-2670(01)84766-8

Schlosser, D., Höfer, C., 2002. Laccase-catalyzed oxidation of Mn^{2+} in the presence of natural Mn^{3+} chelators as a novel source of extracellular H_2O_2 production and its impact on manganese peroxidase. Appl. Environ. Microbiol. 68, 3514–3521. https://doi.org/10.1128/AEM.68.7.3514-3521.2002

Schnetger, B., Dellwig, O., 2012. Dissolved reactive manganese at pelagic redoxclines (part I): A method for determination based on field experiments. Journal of Marine Systems 90, 23–30. https://doi.org/10.1016/j.jmarsys.2011.08.006

Sheriff, T.S., Carr, P., Coles, S.J., Hursthouse, M.B., Lesin, J., Light, M.E., 2004. Structural studies on manganese(III) and manganese(IV) complexes of tetrachlorocatechol and the catalytic reduction of dioxygen to hydrogen peroxide. Inorganica Chimica Acta 357, 2494–2502. https://doi.org/10.1016/j.ica.2003.09.032

Stone, A.T., 1987. Microbial metabolites and the reductive dissolution of manganese oxides: Oxalate and pyruvate. Geochimica et Cosmochimica Acta 51, 919–925. https://doi.org/10.1016/0016-7037(87)90105-0

Stone, A.T., Morgan, J.J., 1984. Reduction and dissolution of manganese(III) and manganese(IV) oxides by organics. 2. Survey of the reactivity of organics. Environ. Sci. Technol. 18, 617–624.

Sun, B., Guan, X., Fang, J., Tratnyek, P.G., 2015. Activation of manganese oxidants with bisulfite for enhanced oxidation of organic contaminants: The involvement of Mn(III). Environ. Sci. Technol. 49, 12414–12421. https://doi.org/10.1021/acs.est.5b03111

Sunda, W.G., Huntsman, S.A., 1988. Effect of sunlight on redox cycles of manganese in the southwestern Sargasso Sea. Deep-Sea Research Part A-Oceanographic Research Papers 35, 1297–1317.

Sunda, W.G., Huntsman, S.A., 1987. Microbial oxidation of manganese in a North Carolina estuary1. Limnol. Oceanogr. 32, 552–564. https://doi.org/10.4319/lo.1987.32.3.0552

825 Sunda, W.G., Kieber, D.J., 1994. Oxidation of humic substances by manganese oxides
826 yields low-molecular-weight organic substrates. Nature 367, 62–64.
827 https://doi.org/10.1038/367062a0
828 Sundby, B., 1977. Manganese-rich particulate matter in a coastal marine environment.
829 Nature 270, 417. https://doi.org/10.1038/270417a0
830 Sundby, B., Silverberg, N., 1985. Manganese fluxes in the benthic boundary layer1.
831 Limnology and Oceanography 30, 372–381.
832 https://doi.org/10.4319/lo.1985.30.2.0372
833 Sundby, B., Silverberg, N., Chesselet, R., 1981. Pathways of manganese in an open
834 estuarine system. Geochimica et Cosmochimica Acta 45, 293–307.
835 https://doi.org/10.1016/0016-7037(81)90240-4
836 Tebo, B.M., Emerson, S., 1986. Microbial manganese(II) oxidation in the marine
837 environment: a quantitative study. Biogeochemistry 2, 149–161.
838 https://doi.org/10.1007/BF02180192
839 Tebo, B.M., Emerson, S., 1985. Effect of oxygen tension, Mn(II) concentration, and
840 temperature on the microbially catalyzed Mn(II) oxidation rate in a marine fjord.
841 Appl. Environ. Microbiol. 50, 1268–1273.
842 Trouwborst, R.E., Clement, B.G., Tebo, B.M., Glazer, B.T., Luther, G.W., 2006. Soluble
843 Mn(III) in suboxic zones. Science 313, 1955–1957.
844 Wariishi, H., Valli, K., Gold, M.H., 1992. Manganese(II) oxidation by manganese
845 peroxidase from the basidiomycete *Phanerochaete chrysosporium*. Kinetic
846 mechanism and role of chelators. J. Biol. Chem. 267, 23688–23695.
847 Wright, M.H., Geszvain, K., Oldham, V.E., Luther, G.W.I., Tebo, B.M., 2018. Oxidative
848 formation and removal of complexed Mn(III) by *Pseudomonas* species. Front.
849 Microbiol. 9. https://doi.org/10.3389/fmicb.2018.00560
850 Wuttig, K., Heller, M.I., Croot, P.L., 2013. Reactivity of inorganic Mn and Mn
851 Desferrioxamine B with O_2, O_2^-, and H_2O_2 in seawater. Environ. Sci. Technol. 47,
852 10257–10265. https://doi.org/10.1021/es4016603
853 Xie, H., Aubry, C., Bélanger, S., Song, G., 2012. The dynamics of absorption coefficients
854 of CDOM and particles in the St. Lawrence estuarine system: Biogeochemical and
855 physical implications. Marine Chemistry 128–129, 44–56.
856 https://doi.org/10.1016/j.marchem.2011.10.001
857 Xyla, A.G., Sulzberger, B., Luther, G.W., Hering, J.G., Van Cappellen, P., Stumm, W.,
858 1992. Reductive dissolution of manganese(III, IV) (hydr)oxides by oxalate: the
859 effect of pH and light. Langmuir 8, 95–103. https://doi.org/10.1021/la00037a019
860 Yakushev, E., Pakhomova, S., Sørenson, K., Skei, J., 2009. Importance of the different
861 manganese species in the formation of water column redox zones: Observations
862 and modeling. Marine Chemistry, 10th International Estuarine Biogeochemistry
863 Symposium - “Estuaries in a Changing World” 117, 59–70.
864 https://doi.org/10.1016/j.marchem.2009.09.007
865 Yakushev, E.V., Pollehne, F., Jost, G., Kuznetsov, I., Schneider, B., Umlauf, L., 2007.
866 Analysis of the water column oxic/anoxic interface in the Black and Baltic seas
867 with a numerical model. Marine Chemistry, 9th International Estuarine

Biogeochemistry Symposium Estuaries and Enclosed Seas under Changing Environmental Conditions 107, 388–410. https://doi.org/10.1016/j.marchem.2007.06.003

Zhu, Y., Liang, X., Zhao, H., Yin, H., Liu, M., Liu, F., Feng, X., 2017. Rapid determination of the Mn average oxidation state of Mn oxides with a novel two-step colorimetric method. Anal. Methods 9, 103–109. https://doi.org/10.1039/C6AY02472F

Zouni, A., Witt, H.-T., Kern, J., Fromme, P., Krauss, N., Saenger, W., Orth, P., 2001. Crystal structure of photosystem II from *Synechococcus elongatus* at 3.8 |[angst]| resolution. Nature 409, 739–743. https://doi.org/10.1038/35055589

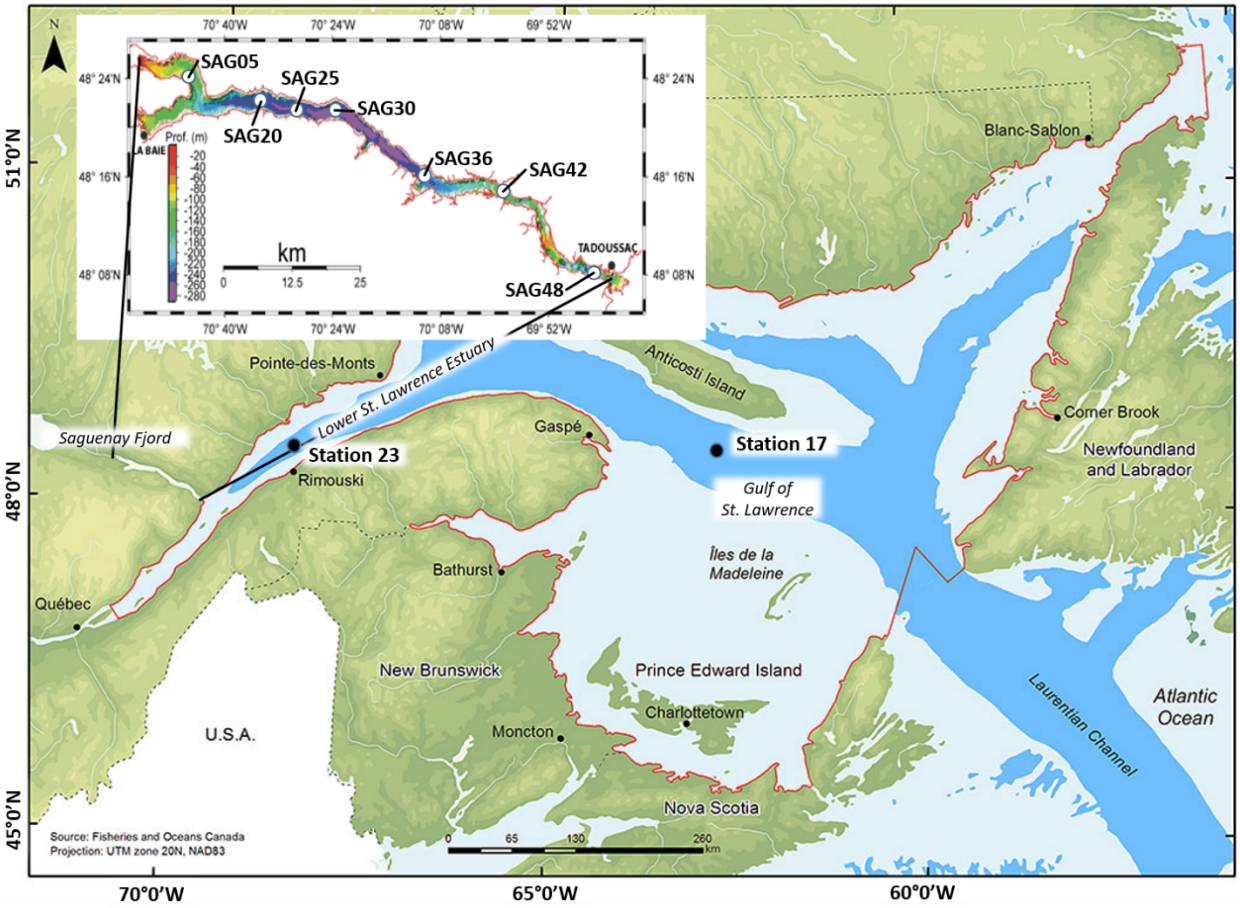

Fig. 1. Location of sampling sites in the St. Lawrence Estuary and Saguenay Fjord (SAG).

Table 1. Locations and water depth of key sampling sites in the St. Lawrence Estuary and Saguenay Fjord (SAG)

Key sample locations	station name	Latitude	Longitude	water depth
Saguenay Fjord	SAG05	48º24.65'N	70º49.50' W	95 m
	SAG30	48˚21.78'N	70˚23.80'W	266 m
	SAG48	48º08.21'N	69º45.15' W	n/a
Lower St. Lawrence Estuary	STN23	48˚42.06'N	68˚39.03'W	340 m
Gulf of St. Lawrence	STN17	48˚58.01'N	63˚06.99'W	406 m

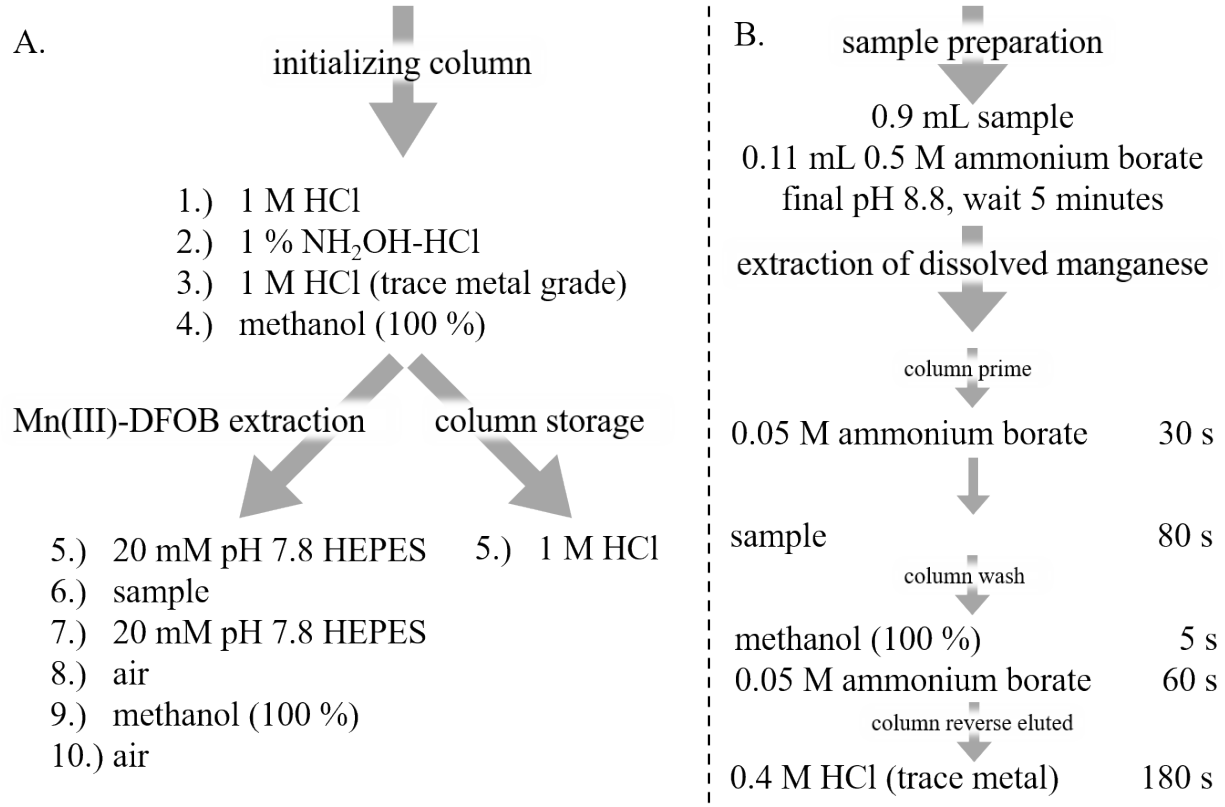

Fig. 2. Chromatography extraction protocols for: A. Mn(III)-DFOB using Waters HLB cartridges (left). The flow rate for reagents and samples through the Waters HLB cartridges was 1 mL min^{-1}. The volume of reagent used at each stage was 4 mL. To remove excess liquid, air was pumped through the cartridges for 1 minute (stage 8) prior to the extraction of Mn(III)-DFOB from the columns using methanol (stage 9). B. Dissolved manganese using AF-Chelate-650M. The AF-Chelate-650M was housed in a 1-cm (18 µL) Global-FIA column incorporated into the FIA-S system (Fig. 3). The flow rates during FIA-S were 0.76 and 0.21 mL min^{-1} for the buffered sample and reagents, respectively.

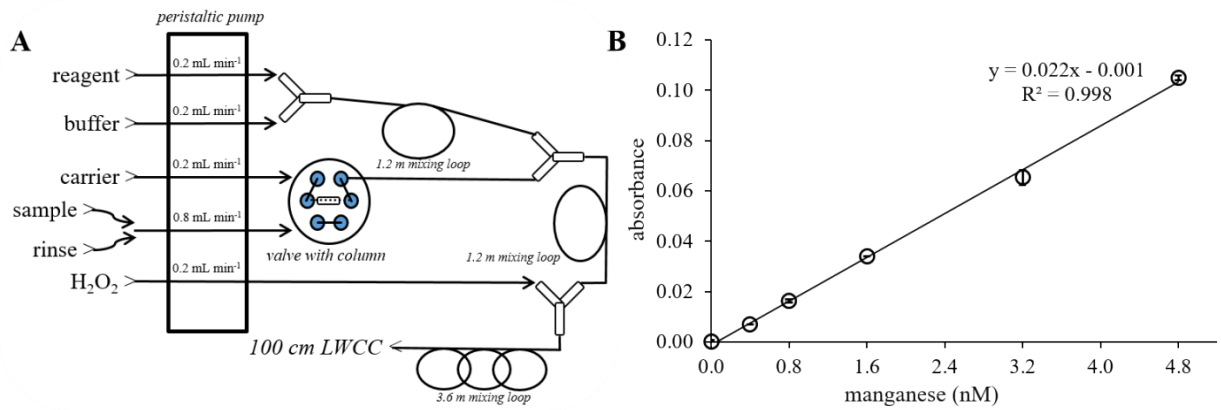

Fig. 3. A. Flow injection analysis – spectrophotometry schematic. The 6-port, 2-way valve holds a 1-cm (18 μL) Global-FIA column. B. Blank corrected calibration curve for oxidized Tiron measured at 424 nm in a 100-cm long wave capillary. Error bars represent the standard deviation of triplicate analyses of the standard.

Table 2. UV-Vis spectrophotometric methods used to quantify the concentrations of Mn(III)-L, based either on their respective molar absorptivity (ε) at the diagnostic wavelength or by colorimetry.

Mn(III)-L complex	ε	Wavelength	reference
Mn(III)-malonate	11.6 $mMol^{-1}$ L cm^{-1}	270 nm	Wariishi et al., (1992)
Mn(III)-pyrophosphate	104 $mMol^{-1}$ L cm^{-1}	480 nm	Archibald and Fridovich (1982)
Mn(III)-citrate	310 Mol^{-1} L cm^{-1}	430 nm	Duke (1947)
Mn(III)-pyruvate	formaldoxime assay		Brewer and Spencer (1971)

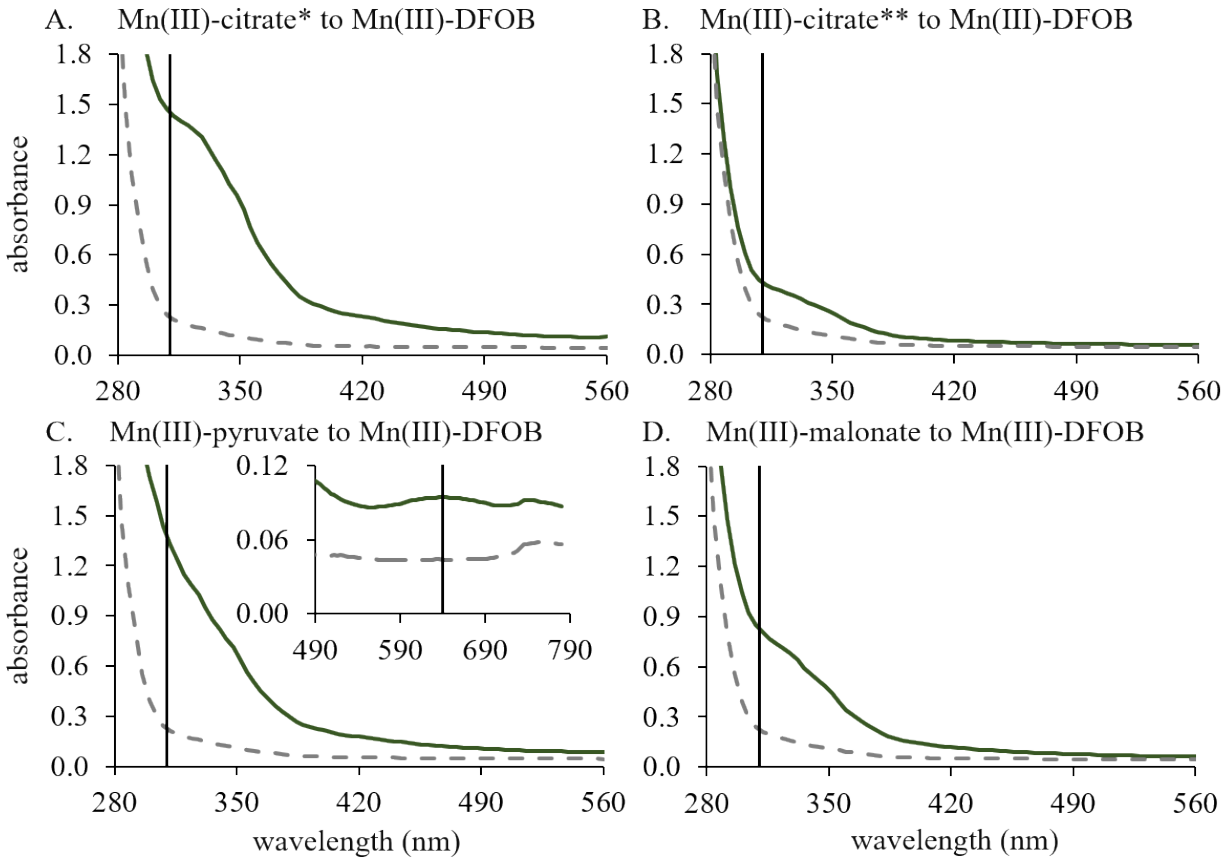

Fig. 4. Formation of Mn(III)-DFOB in seawater. Absorbance spectra before (Mn(III)-L, grey dashed line) and after (Mn(III)-DFOB, dark green solid line) the addition of DFOB to Mn(III)-L in seawater. Panels A and B, Mn(III)-citrate; Panel C, Mn(III)-pyruvate; Panel D, Mn(III)-malonate. Mn(III)-DFOB is characterized by a broad shoulder at 310–320 nm (black vertical line indicates 310 nm at the beginning of the shoulder). Inset Panel C; absorbance peak at 640 nm (indicated by vertical black line) used to quantify Mn(III)-DFOB relative to seawater and seawater with DFOB. Panels A and B; Mn(III)-citrate* was formed through the addition of sodium citrate to a MnO_x slurry and Mn(III)-citrate** was formed through the oxidation of manganese(II) at pH 9 in the presence of sodium citrate (Supplementary Material).

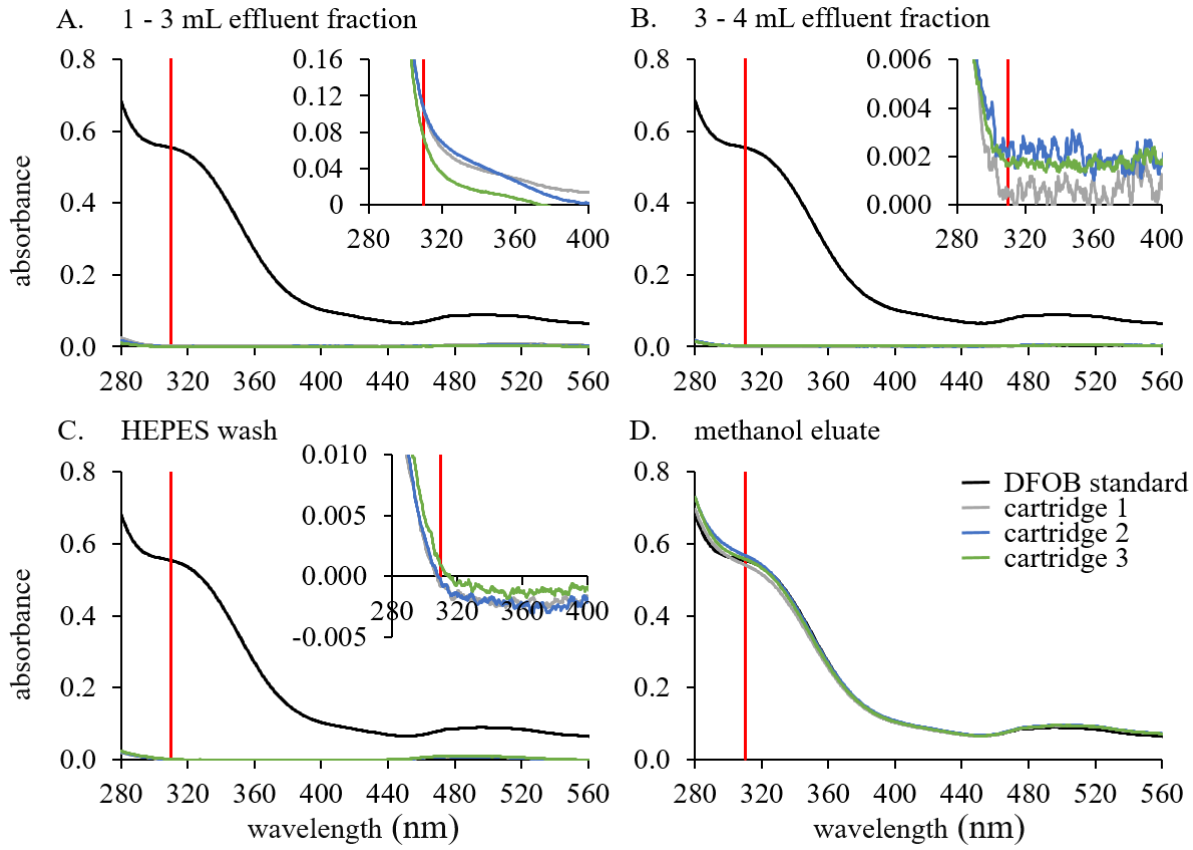

Fig. 5. Extraction of Mn(III)-DFOB. Absorbance spectra of collected fractions from three separate cartridges (grey, blue and green spectra) as a 269 μM Mn(III)-DFOB (black spectrum) standard was passed through 225 mg Water HLB cartridges. Mn(III)-DFOB is characterized by a broad shoulder at 310–320 nm (red vertical line indicates 310 nm at the beginning of the shoulder). Panels A to D and insets B and C were measured on a 1-cm cell and are compared to the original Mn(III)-DFOB standard. Inset Panel A: the absorbance spectra of the effluents from each cartridge measured in a 100-cm LWCC. Fractions collected: 1-3 mL fraction of the experimental effluent (first 1 mL was discarded; Panel A), the 3-4 mL fraction (Panel B), the HEPES wash (Panel C), and the methanol eluate (Panel D).

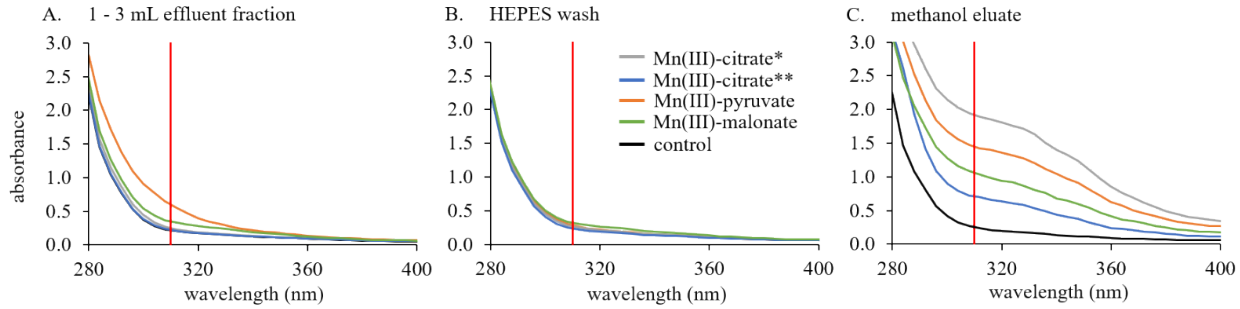

Fig. 6. Extraction of Mn(III)-DFOB. Absorbance spectra, measured in a 1-cm cell, of fractions collected during extraction of Mn(III)-DFOB from seawater. Mn(III)-DFOB, characterized by a broad shoulder over the range 310-320 nm (310 nm indicated by the vertical red line), is only present in the methanol eluate, Panel C. Fractions collected: 1-3 mL fraction of the experimental effluent (first 1 mL was discarded; Panel A), the HEPES wash (Panel B), and methanol eluate (Panel C). Mn(III)-citrate* was formed through the addition of sodium citrate to a MnO_x slurry and Mn(III)-citrate** was formed through the oxidation of manganese(II) at pH 9 in the presence of sodium citrate (Supplementary Material).

Table 3. Comparison between Mn(III)-DFOB formed in seawater (Fig. 4) and the methanol elute (Fig. 6). Mn(III)-DFOB concentrations (μM) were calculated using absorption at 310 nm. Methanol elution volume was 50 % of the seawater sample volume and, thus, the concentration of Mn(III)-DFOB in the eluate was doubled to calculate the recovered concentration.

Mn(III)-L_{DFOB} source	seawater concentration	recovered concentration	recovery (%)
Mn(III)-citrate*	404	386	95
Mn(III)-citrate**	68	69	101
Mn(III)-pyruvate	313‡	299	96
Mn(III)-malonate	198	184	93

* Mn(III)-citrate was formed from reduction of MnOx by citrate (excess MnO_x removed through filtration). ** Mn(III)-citrate was formed from the oxidation of manganese(II) in the presence of citrate (excess manganese(II)). ‡ Concentration calculated from absorbance and molar absorptivity at 640 nm.

Table 4 Physicochemical measurements and manganese concentrations for samples collected in the St. Lawrence Estuary and the Saguenay Fjord (potential density, σ_θ; *in-situ* pH on the total proton scale, $pH_{t\text{-}is}$), any processing of samples, i.e. the addition of DFOB, took place post filtration. The MnO_2 error is ±5 %, whereas the reproducibility of standards was ±2 %. The Mn(III)-L_{DFOB} error is the higher of either the relative error based on duplicate analyses during FIA-S or that calculated from the percentage error from triplicate analyses at each site. The dMn_T error is the co-variance based on replicate analyses of the standards. Samples for dMn_T at Station 23, *italicized*, are taken from Oldham et al. (2017b) (see text for reference). MnO_2 measurements in **bold** are referred to explicitly in the discussions, Section 4.2.

depth (m)	Salinity	temperature (°C)	σ_θ	$pH_{t\text{-}is}$	O_2 (μM)	MnO_2 (nM)	dMn_T (nM)	Mn(III)-L_{DFOB} (nM)
Gulf of St. Lawrence, Station 17								
3	29.88	5.70	22.3	7.83	142	1.6 ± 0.1	-	2.2 ± 0.09
21	31.6	12.0	25.1	8.06	283	1 ± 0.1	-	1.1 ± 0.04
60	32.24	2.87	26.1	8.10	346	2.3 ± 0.1	-	0.77 ± 0.03
100	32.67	-0.60	26.5	8.02	331	3.4 ± 0.2	-	1.0 ± 0.04
150	33.27	-0.09	26.8	7.98	296	2.3 ± 0.5	-	0.79 ± 0.03
200	34.02	2.45	27.2	7.93	233	2 ± 0.3	-	BDL
250	34.3	5.22	27.5	7.86	180	**9.5 ± 0.5**	-	0.73 ± 0.03
300	34.63	5.38	27.8	7.74	114	**16 ± 0.3**	-	0.86 ± 0.03
350	34.79	5.87	28.1	7.78	118	**21 ± 0.1**	-	0.76 ± 0.1
390	34.81	5.74	28.2	7.82	138	**52 ± 0.3**	-	1.1 ± 0.2
Lower St. Lawrence Estuary, Station 23								
3	27.76	7.89	21.6	8.03	339	4.2 ± 0.2	*81 ± 3*	2.0 ± 0.08
20	30.02	4.15	23.8	7.90	277	18 ± 0.2	*86 ± 1*	0.7 ± 0.1
50	31.86	0.8	25.5	7.95	304	11 ± 0.6	*108 ± 27*	1.4 ± 0.06
80	32.25	0.32	25.9	7.93	299	9.2 ± 0.2	*126 ± 16*	1.3 ± 0.05
100	32.89	1.55	26.3	7.83	235	24 ± 1.0	*103 ± 5*	1.0 ± 0.06
150	33.73	3.69	26.8	7.71	134	55 ± 0.2	*253 ± 6*	0.95 ± 0.07
200	34.16	4.65	27.0	7.69	83	**170 ± 9**	*222 ± 5*	0.87 ± 0.04
250	34.33	5.08	27.1	7.64	69	**300 ± 2**	*300 ± 14*	0.7 ± 0.03

300	34.46	5.33	27.2	7.64	60	**470 ± 3**	*295 ± 10*	2.7 ± 0.1
340	34.49	5.41	27.2	7.65	55	**1070 ± 11**	*295 ± 17*	1.9 ± 0.2
Saguenay Fjord, Station SAG30								
3	15	11.3	11.1	7.83	297	4.4 ± 0.2	54 ± 2	3.4 ± 0.2
10	24.83	7.15	19.4	7.84	287	5.9 ± 0.3	39 ± 2	2.6 ± 0.2
20	28.17	5.38	22.2	7.90	298	14 ± 0.7	23 ± 1	2.7 ± 0.2
50	29.12	3.56	23.2	7.89	293	18 ± 0.9	21 ± 1	2.7 ± 0.1
100	29.61	2.55	23.6	7.87	281	13 ± 0.7	32 ± 1	-
125	29.87	2.84	23.8	7.87	276	16 ± 0.8	64 ± 3	2.5 ± 0.1
150	30.03	2.2	24.0	7.84	272	18 ± 0.9	75 ± 3	2.7 ± 0.1
200	30.6	1.86	24.5	7.79	251	22 ± 1.1	206 ± 8	4.0 ± 0.2
250	30.83	1.79	24.6	7.74	230	13 ± 0.7	489 ± 13	3.8 ± 0.4
Saguenay Fjord, Station SAG05								
2	3.5	14.1	1.5	7.72	298	20 ± 1.0	45 ± 2	0.88 ± 0.04
5	14.3	10.4	11.6	7.80	291	7.5 ± 0.4	56 ± 2	0.52 ± 0.02
10.4	26.4	6.23	20.8	7.89	290	9 ± 0.5	34 ± 1	0.78 ± 0.03
20	27.9	3.7	22.1	7.88	285	12 ± 0.6	51 ± 2	1.4 ± 0.1
60	29.1	1.62	23.3	7.82	272	9.9 ± 0.5	140 ± 5	1.8 ± 0.1
85	29.4	1.61	23.5	7.80	268	12 ± 0.6	180 ± 7	0.41 ± 0.02
Saguenay Fjord, surface transect								
SAG05 (5m)	14.3	14.1	-	-	-	7.5 ± 0.3	56 ± 2	0.52 ± 0.03
SAG20 (2m)	12.2	11.4	-	-	-	4.5 ± 0.3	54 ± 2	3.2 ± 0.1
SAG25 (2m)	11	12	-	-	-	4.3 ± 0.3	54 ± 2	7.3 ± 0.3
§SAG30 (3m)	15	11.3	-	-	-	4.4 ± 0.3	54 ± 2	3.4 ± 0.2
SAG36 (3m)	12.2	11.8	-	-	-	0.96 ± 0.04	57 ± 2	5.4 ± 0.2
SAG42 (2m)	13.5	11.3	-	-	-	1.2 ± 0.03	54 ± 2	7.5 ± 0.3
SAG48 (3m)	14.5	10.3	-	-	-	1.3 ± 0.01	55 ± 2	5.5 ± 0.2

991 §, sample collected approximately 24-hours prior; -, parameter not measured for those samples; BDL, sample below the detection
992 limit. The underlined salinity values were determined in the laboratory by argentimetric titration; all other salinities taken from the
993 CTD sensor.

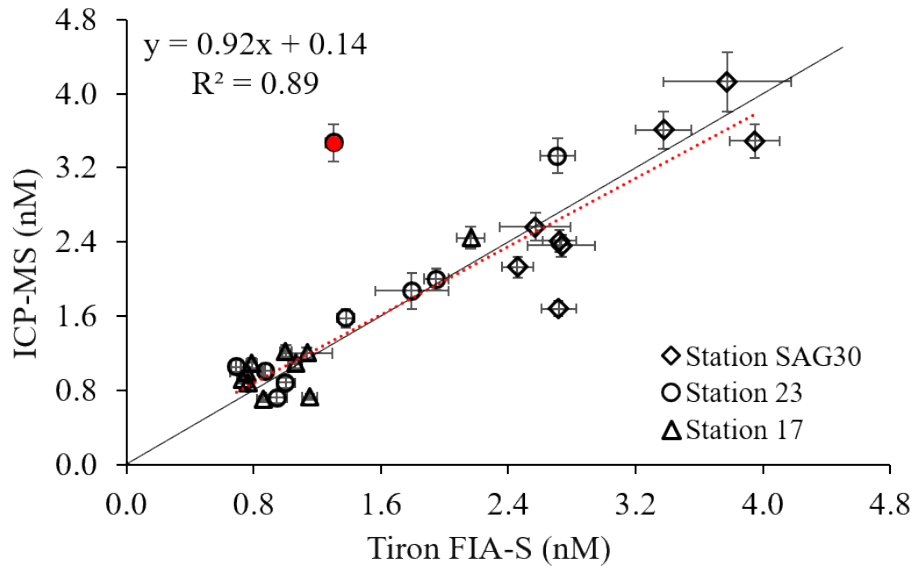

Fig. 7. Mn(III)-DFOB in methanol extracted from St. Lawrence Estuary waters and measured by ICP-MS compared to the Tiron FIA-S measurements. The red dotted line is the linear regression of all data except for Station 23, 200m, (red dot; the ICP-MS over-recovery of 266 % was a statistical outlier > ±3 × standard deviation of all recoveries). The black line is the 1:1 line.

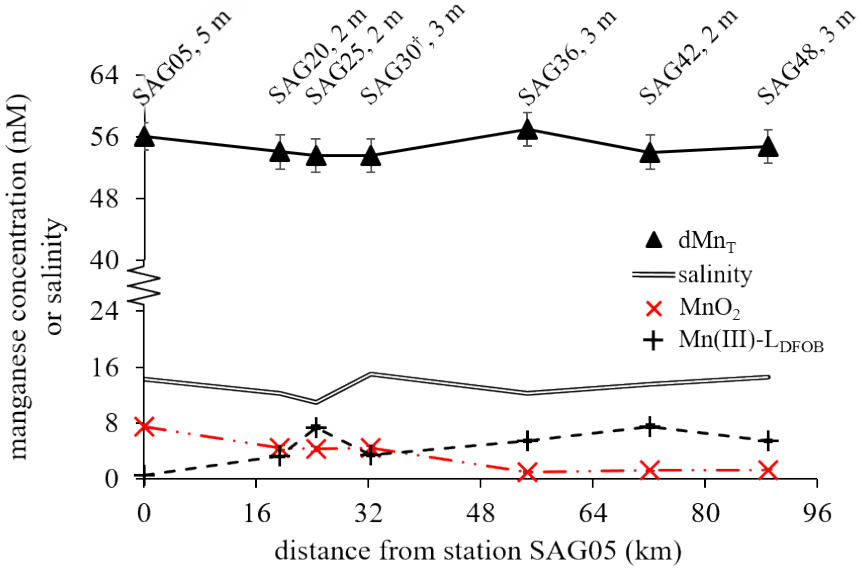

Fig. 8. Concentrations of manganese species, and variation in salinity, throughout the Saguenay Fjord transect. Station name is represented by SAG## followed by sampling depth in meters. The SAG30† sample was collected 24 h prior to all other samples. Note that the y-axis is compressed between 24-40 nM to allow for better visualization of the data.

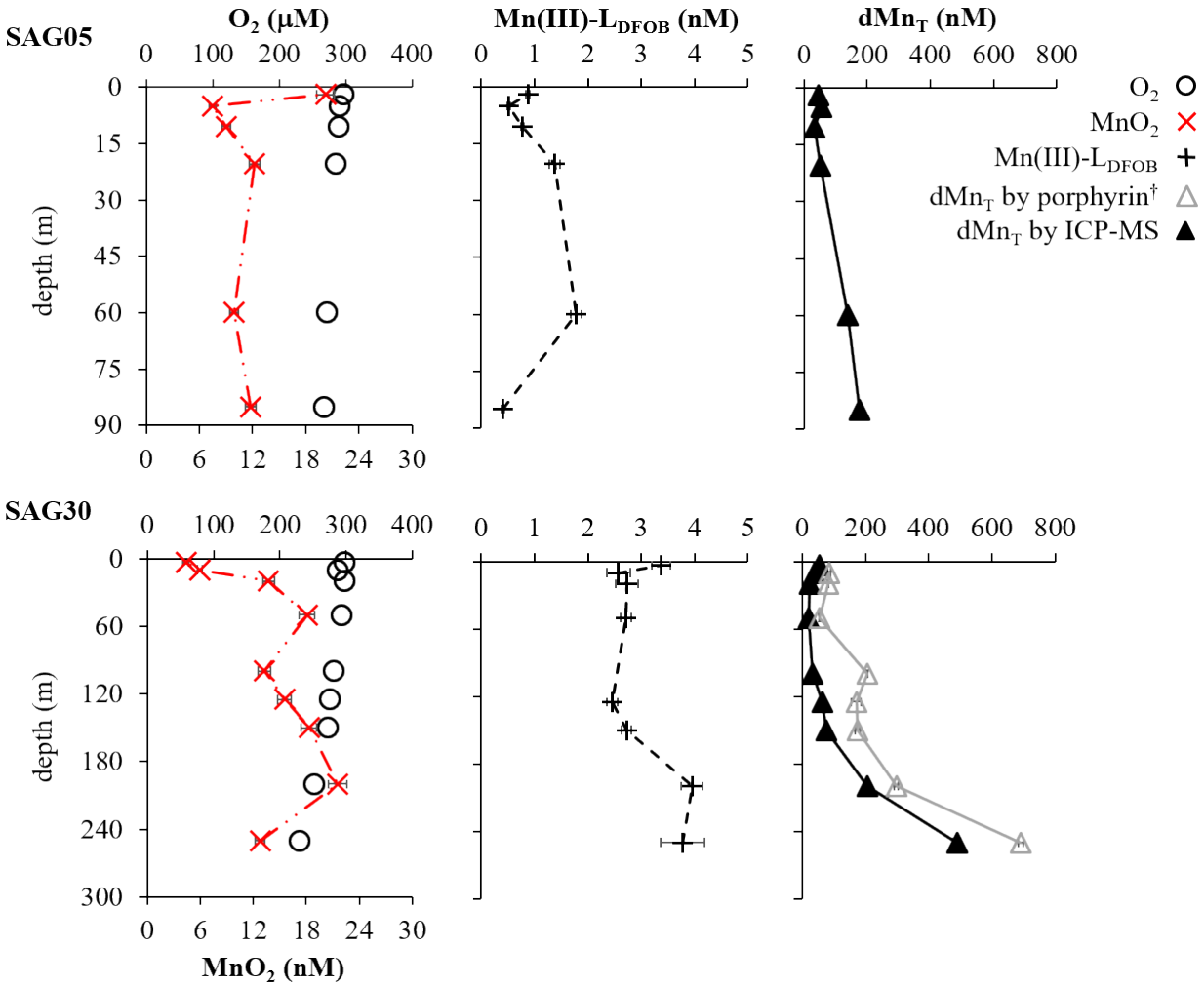

Fig. 9. Depth profiles for dissolved oxygen and manganese species sampled at stations SAG05 and SAG30 in the Saguenay Fjord. Samples for dMn_T, as measured by the porphyrin technique for SAG30, are taken from Oldham et al. (2017b).

1047

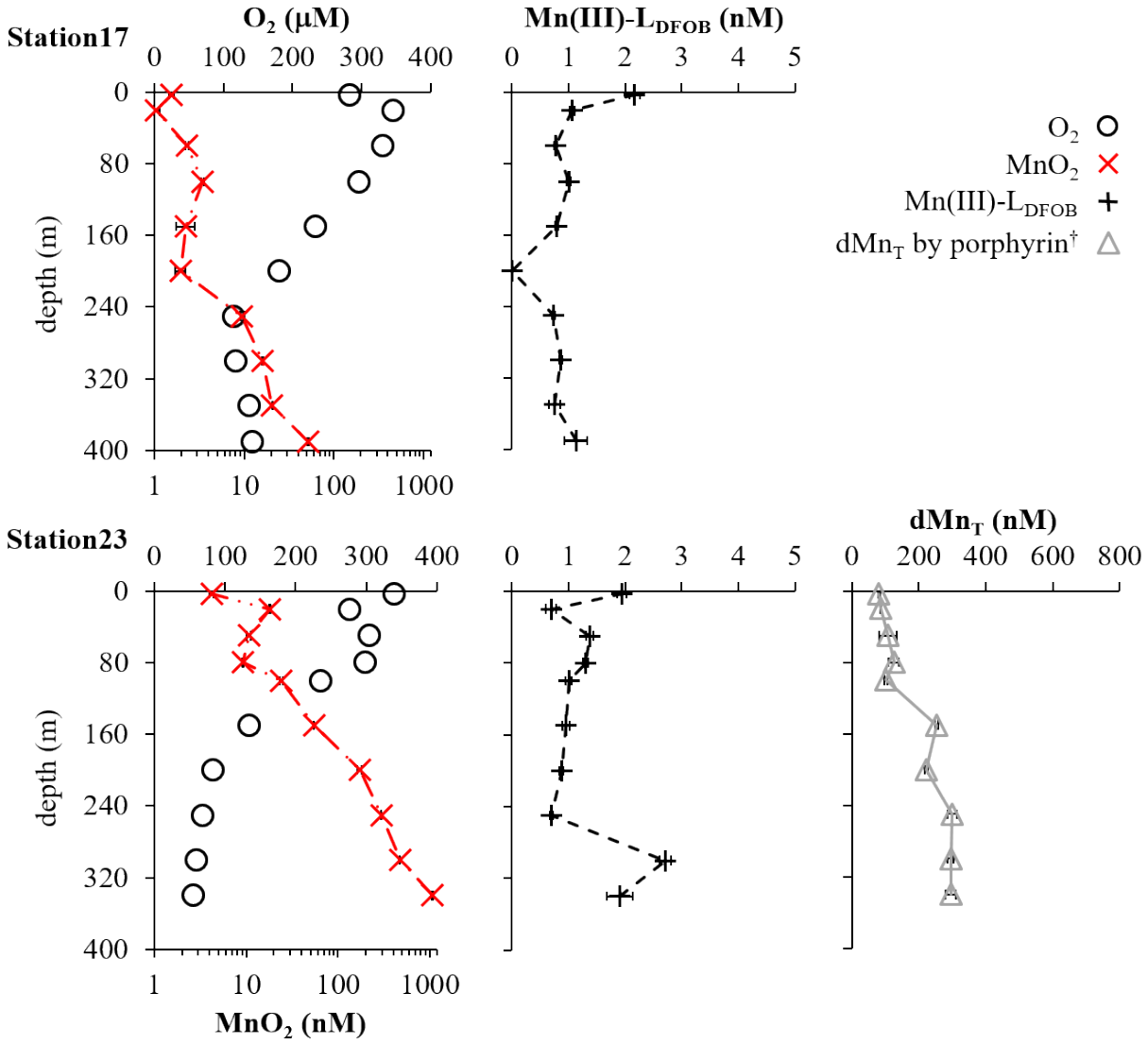

1048

1049 Fig. 10. Depth profiles for dissolved oxygen and manganese species at Stations 17 and 23 in the
1050 Gulf of St Lawrence and Lower St. Lawrence Estuary. MnO_2 concentrations are presented on a
1051 logrithmic scale. Samples for dMn_T for Station 23 are taken from Oldham et al. (2017b).